UNIVERSIDAD DE INVESTIGACIÓN DE TECNOLOGÍA EXPERIMENTAL YACHAY

Escuela de Ciencias Químicas e Ingeniería

TÍTULO: Theoretical study of interaction of COVID-19 palliative chlorine dioxide with hemoglobin analogs

Trabajo de integración curricular presentado como requisito para la obtención de título de Químico

Autor:

Pamela Alejandra Andrade Mina

Tutor:

Juan Pablo Saucedo Vázquez, PhD

Urcuquí, Enero 2022

Urcuquí, 21 de enero de 2022

SECRETARÍA GENERAL
(Vicerrectorado Académico/Cancillería)
ESCUELA DE CIENCIAS QUÍMICAS E INGENIERÍA
CARRERA DE QUÍMICA
ACTA DE DEFENSA No. UITEY-CHE-2022-00022-AD

A los 21 días del mes de enero de 2022, a las 12:30 horas, de manera virtual mediante videoconferencia, y ante el Tribunal Calificador, integrado por los docentes:

Presidente Tribunal de Defensa	Dr. FERREIRA DE MENEZES AREIAS , FILIPE MIGUEL , Ph.D.
Miembro No Tutor	Dra. LOPEZ GONZALEZ, FLORALBA AGGENY , Ph.D.
Tutor	Dr. SAUCEDO VAZQUEZ, JUAN PABLO , Ph.D.

El(la) señor(ita) estudiante **ANDRADE MINA, PAMELA ALEJANDRA**, con cédula de identidad No. **1004158919**, de la **ESCUELA DE CIENCIAS QUÍMICAS E INGENIERÍA**, de la Carrera de **QUÍMICA**, aprobada por el Consejo de Educación Superior (CES), mediante Resolución **RPC-SO-39-No.456-2014**, realiza a través de videoconferencia, la sustentación de su trabajo de titulación denominado: **THEORETICAL STUDY OF THE INTERACTION OF COVID-19 PALLIATIVE CHLORINE DIOXIDE WITH HEMOGLOBIN ANALOGS**, previa a la obtención del título de **QUÍMICO/A**.

El citado trabajo de titulación, fue debidamente aprobado por el(los) docente(s):

Tutor	Dr. SAUCEDO VAZQUEZ, JUAN PABLO , Ph.D.

Y recibió las observaciones de los otros miembros del Tribunal Calificador, las mismas que han sido incorporadas por el(la) estudiante.

Previamente cumplidos los requisitos legales y reglamentarios, el trabajo de titulación fue sustentado por el(la) estudiante y examinado por los miembros del Tribunal Calificador. Escuchada la sustentación del trabajo de titulación a través de videoconferencia, que integró la exposición de el(la) estudiante sobre el contenido de la misma y las preguntas formuladas por los miembros del Tribunal, se califica la sustentación del trabajo de titulación con las siguientes calificaciones:

Tipo	Docente	Calificación
Tutor	Dr. SAUCEDO VAZQUEZ, JUAN PABLO , Ph.D.	10,0
Presidente Tribunal De Defensa	Dr. FERREIRA DE MENEZES AREIAS , FILIPE MIGUEL , Ph.D.	10,0
Miembro Tribunal De Defensa	Dra. LOPEZ GONZALEZ, FLORALBA AGGENY , Ph.D.	10,0

Lo que da un promedio de: **10 (Diez punto Cero)**, sobre 10 (diez), equivalente a: **APROBADO**

Para constancia de lo actuado, firman los miembros del Tribunal Calificador, el/la estudiante y el/la secretario ad-hoc.

Certifico que *en cumplimiento del Decreto Ejecutivo 1017 de 16 de marzo de 2020, la defensa de trabajo de titulación (o examen de grado modalidad teórico práctica) se realizó vía virtual, por lo que las firmas de los miembros del Tribunal de Defensa de Grado, constan en forma digital.*

ANDRADE MINA, PAMELA ALEJANDRA
Estudiante

Dr. FERREIRA DE MENEZES AREIAS , FILIPE MIGUEL , Ph.D.
Presidente Tribunal de Defensa

FILIPE MIGUEL FERREIRA DE MENEZES AREIAS
Firmado digitalmente por FILIPE MIGUEL FERREIRA DE MENEZES AREIAS
Fecha: 2022.01.25 20:00:01 -05'00'

Dr. SAUCEDO VAZQUEZ, JUAN PABLO , Ph.D.
Tutor

JUAN PABLO SAUCEDO VAZQUEZ
Firmado digitalmente por JUAN PABLO SAUCEDO VAZQUEZ
Nombre de reconocimiento (DN): c=EC, o=BANCO CENTRAL DEL ECUADOR, ou=ENTIDAD DE CERTIFICACION DE INFORMACION-ECIBCE, l=QUITO, serialNumber=0000260799, cn=JUAN PABLO SAUCEDO VAZQUEZ
Fecha: 2022.01.25 10:18:48 -05'00'

FLORALBA AGGENY LOPEZ GONZALEZ

Digitally signed by FLORALBA AGGENY LOPEZ GONZALEZ
Date: 2022.01.25 09:03:55 -05'00'

Dra. LOPEZ GONZALEZ, FLORALBA AGGENY , Ph.D.
Miembro No Tutor

YEPEZ MERLO, MARIELA SOLEDAD
Secretario Ad-hoc

Firmado electrónicamente por:
**MARIELA
SOLEDAD YEPEZ
MERLO**

AUTORÍA

Yo, PAMELA ALEJANDRA ANDRADE MINA, con cédula de identidad 1004158919, declaro que las ideas, juicios, valoraciones, interpretaciones, consultas bibliográficas, definiciones y conceptualizaciones expuestas en el presente trabajo; así cómo, los procedimientos y herramientas utilizadas en la investigación, son de absoluta responsabilidad de el/la autor (a) del trabajo de integración curricular. Así mismo, me acojo a los reglamentos internos de la Universidad de Investigación de Tecnología Experimental Yachay.

Urcuquí, Octubre 2021.

Pamela Alejandra Andrade Mina
CI: 1004158919

AUTORIZACIÓN DE PUBLICACIÓN

Yo, PAMELA ALEJANDRA ANDRADE MINA, con cédula de identidad 1004158919, cedo a la Universidad de Investigación de Tecnología Experimental Yachay, los derechos de publicación de la presente obra, sin que deba haber un reconocimiento económico por este concepto. Declaro además que el texto del presente trabajo de titulación no podrá ser cedido a ninguna empresa editorial para su publicación u otros fines, sin contar previamente con la autorización escrita de la Universidad.

Así mismo, autorizo a la Universidad que realice la digitalización y publicación de este trabajo de integración curricular en el repositorio virtual, de conformidad a lo dispuesto en el Art. 144 de la Ley Orgánica de Educación Superior.

Urcuquí, Octubre 2021.

Pamela Alejandra Andrade Mina
CI: 1004158919

Acknowledgements

I would like to express my infinite gratitude to all and each one of the professors, who mentored me during my career. Thanks for the patience, and for the time spend even in extracurricular classes, for motivating me to do science, and most important for making me believe that I can do it. Especially, I am grateful to professor Juan Pablo Saucedo, who was my guide since my first day class in Yachay, and whom I admire a lot for his simplicity and the excellent professor he is. Furthermore, I want to thank professor Terencio Tibaulth, I could not have done it without his help and advices.

On the other hand, a fundamental part of my life is my family, never be enough to thanks for all the support that they give me. Mom, you show me to never give up. Dad, you are the best example of hard work, brother and sister, thanks for listening to me in the worst situations, take my hand and get up. To my aunt, Lucia, grateful for your unconditional help, thank you for always being there for me. All of you, and your lessons means a lot to me.

I feel blessed to had met special people, my dear friends, Emerson, Maylin and Ali, you be of my career an unforgettable experience, you took me out of my comfort zone and made me see that taking risks to grow professionally is essential, and it is better to do it with friends. Thanks for all you support, specially to Ali for help me with her cluster account. I could not miss the opportunity to thank my friends Ivette and Moises too for always be ready to help me. Finally thanks a lot to my friends, who became in my second family, Mauricio, Pilar, Luis Miguel, Rocío and Maikol.

Pamela Andrade

Dedicatory

To my parents and brothers

To my dear friends

To people who believe in me

To all people who believe chlorine dioxide is the palliative against illness

Pamela Andrade

Resumen

El uso de dióxido de cloro (ClO_2) ha tomado protagonismo como un paliativo para combatir enfermedades virales como el COVID-19. A pesar de que las organizaciones y entes regulatorios no han avalado su uso y han advertido de sus posibles efectos dañinos en la salud, su consumo sigue siendo popular entre la población. El ClO_2, en solución acuosa produce subproductos como cloritos y puede actuar como un potente agente oxidante hacia diferentes biomoléculas que juegan roles biológicos importantes en el ser humano, tal es el caso de las hemoproteínas cuyo sitio activo, el grupo hemo, alberga un átomo de hierro en el que el control de su ambiente químico y su estructura electrónica son muy importantes para que sus funciones biológicas no sean alteradas. Por ello, este trabajo tiene como objetivo estudiar las interacciones del ClO_2 y su el ion clorito ClO_2^- con el grupo hemo-b, así como comparar los cambios en las propiedades estructurales y electrónicas que se producen por efecto de dichas interacciones. Para llevar a cabo este estudio se ha utilizado herramientas computacionales que permiten predecir, el comportamiento de los complejos de interés. A través de la teoría funcional de densidad DFT y el funcional B3LYP se realizó la optimización de geometría de los complejos, así como también se estudiaron las propiedades estructurales y electrónicas. Por otro lado, se realizó un estudio experimental de la interacción de dichos derivados clorados con la enzima bifuncional catalasa peroxidasa de *Neurospora crassa*, CAT2. Dicha enzima se utilizó como modelo estructural debido a que contiene un grupo prostético hemo-b en su sitio activo.

Los resultados computacionales obtenidos demuestran que los ligantes ClO_2 y ClO_2^- se coordinan al hierro mediante el átomo de oxígeno y con una energía menor a la forma oxigenada. Aedmas, los ligantes H_2O, O_2, ClO_2 y ClO_2 producen una distorsión de la geometría octaédrica que está en oncordancia con lo reportado en la literatura. El análisis poblacional de Mulliken muestra un cambio significativo en la carga del hierro. Finalmente, del análisis experimental de interacción de la enzima CAT-2 con una disolución comercial de dióxido de cloro, se documentaron cambios espectrales significativos que revelan la degradación del grupo hemo. Ambos tipos de resultados apoyan la hipótesis de este trabajo, en el sentido de que el uso de dióxido de cloro como agente paliativo para el tratamiento de COVID-19 puede causar alteraciones importantes en el funcionamiento de biomoléculas relevantes para el cuerpo humano como la hemoglobina.

Palabras clave: dióxido de cloro, clorito, hemo-b, COVID-19.

Abstract

The use of chlorine dioxide (ClO_2) has taken an important role as a palliative to combat viral diseases such as COVID-19. Even though organizations and regulatory entities have not endorsed its use and have warned of its possible harmful effects on health, its consumption continues to be popular among the population. ClO_2 in aqueous solution gradually produces by-products such as chlorites and can act as a powerful oxidizing agent of different biomolecules that play important biological roles in humans, such is the case of hemoproteins whose active site, the heme group, contains an iron atom in which the control of its chemical environment and its electronic structure are very important for their biological functions. For this reason, this work aims to study the interactions of ClO_2 and its main derivative, the chlorite ion ClO_2^- with the heme-b group, as well as to compare the changes in structural and electronic properties that occur because of these interactions. To carry out this study, computational tools have been used to predict the behavior of the complexes of interest. Through the DFT density functional theory and the B3LYP functional, the geometry of the complexes was optimized, as well as the structural and electronic properties. On the other hand, an experimental study of the interaction of such chlorinated derivatives with the bi-functional enzyme catalase peroxidase from *Neurospora crassa*, CAT2, was carried out. This enzyme was used as an structural model because it contains a heme-b prosthetic group in its active site.

The computational results obtained show that the ClO_2 and ClO_2^- ligands coordinate to iron through the oxygen atom and with less energy than the oxygenated form. Regarding its geometry, it is evident that in the presence of the ligands H_2O, O_2, ClO_2 and ClO_2^- there is a distortion of the octahedral geometry that is in accordance with that reported in the literature; furthermore, the Mulliken population analysis shows a significant change in iron charge. Finally, from the experimental analysis of the interaction of the CAT-2 enzyme with a commercial solution of chlorine dioxide, significant spectral changes were documented, demonstrating the degradation of the heme group caused by such interaction. Both types of results support the hypothesis of this work, in the sense that the use of chlorine dioxide as a palliative agent for the treatment of COVID-19 can cause important alterations in the functioning of biomolecules relevant to the human body such as hemoglobin.

Keywords: chlorine dioxide, chlorite, heme-b, COVID-19.

Contents

List of Figures

List of Tables

Chapter 1

Introduction

Faced with the current global health problem going through humanity due to the COVID-19 disease that has left around millions of deaths [1], public health organizations and the scientific community have joined forces to try to get vaccines, medicines and security equipment that can act to mitigate the spread of the disease and its effects; however, in this attempt, the time devoted to the study and development of these drugs has represented one of the most important problems.

The necessity, and the emergency of getting the cure for the disease, have opened the doors to the use and abuse of palliative treatments of the easy access to the population. This is the case of the chemical substance, chlorine dioxide. The use of this substance as a treatment against COVID-19 has been broadcast since people, who assure to have healed until health professionals [2].

However, the use of chlorine dioxide has been a dilemma because some scientists have assured that although this substance can act against the SARS-CoV-2 virus, it should be considered what are the adequate conditions in which it can be used without negative health effects, especially differentiating between *in vitro* and *in vivo* studies. In the latter case, it is important to take into account that because chlorine dioxide is not a selective substance, its consumption can bring health complications that, far from counteracting one disease, can be the trigger for others [3].

In this sense, due to the well know oxidative properties of the dioxide chloride, it could be a potential agent that oxidizes to the heme-proteins as hemoglobin, in particular in the heme group. As a result, it can produce the formation of methemoglobin which becomes a health problem, due to the loss of coordination to oxygen difficult to transport it from blood to tissues. Thus, abnormal amounts of methemoglobinemia, cause a functional "anemia" with cyanosis (due to the ability to the reduced blood supply to carry oxygen) [4].

1.1   Problem Statement

For many years, chlorine dioxide has been used extensively in the food industry up to water treatment. Today, chloride dioxide has emerged as a possible disease treatment due to its microbicidal property. Based on this fact, many people around the world are using chlorine dioxide as a palliative agent against COVID-19. However, ingesting chlorine dioxide could have a significant adverse effect on human health. Although regulatory agencies and agents have spoken out about the harmful effects of ingesting the chlorine dioxide solution, and despite the lack of scientific evidence of a coronavirus cure, many people continue with their ingestion supported by a few promoters. Therefore, some cases of mortality have been recorded.

One of the health problems that dioxide chloride can develop is related to the changes in the functionality of the heme-b group present in the hemoglobin. It is due to the oxidant properties of this molecule to become ferrous ion in their ferric form, provoking that hemoglobin loses the biological property to catch and release oxygen to the tissues [4]. For that reason, this work focuses on the study of the interactions of chlorine dioxide, or its derivatives formed in aqueous solution such as chlorite with heme-b models from both theoretical and experimental point of view.

1.2 Objectives

1.2.1 General Objective

To identify and to analyze interactions between chlorine dioxide and chlorite with analogous of hemoglobin containing the heme-b group, through computational methods and experimental studies, which let us to understand the nature of such interactions, and their affections in the functionality of heme group

1.2.2 Specific Objectives

- To compare the stability of the heme-b system under the presence of different types of ligands both naturally observed as water and dioxygen and toxic derivatives as chlorine dioxide, chloride ion, and chlorite through computational calculations.

- To analyze the change in the electronic distribution by the effect of the ligands through the Mulliken Population

- To isolate and purify the enzyme catalase-peroxidase (CAT-2) to use it as an experimental heme-b model.

- To evaluate the reactivity of CAT-2 heme-b enzyme with a commercial sample of chlorine dioxide through UV-Vis spectroscopy analysis

Chapter 2

Theoretical Background

2.1   Chlorine Dioxide

The discovery of chlorine dioxide is attributed to the British scientist Humprey Davy, who in 1814 achieved synthesis through the reaction of sulphuric acid ($H2SO4$) and potassium chlorate ($KClO3$). More alternatives to synthesize chlorine dioxide are known, and the two more commons are by the reaction of sodium chlorite with chlorine gaseous or by the reaction of sodium chlorite with sodium hypochlorite and sulfuric acid [5]. As we can see in equations 2.1 and 2.2.

$$2NaClO_2 + Cl_2 \rightarrow 2ClO_2 + 2NaCl \tag{2.1}$$

$$2NaClO_2 + NaOCl + H_2SO_4 \rightarrow 2ClO_2 + NaCl + Na_2SO_4 + H_2O \tag{2.2}$$
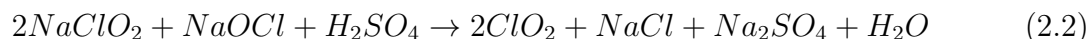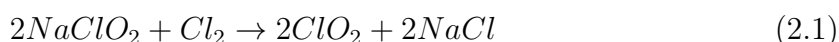
Since chlorine dioxide was discovered, many studies around its efficacy in the treatment of illness have been realized. The use of chlorine dioxide as a palliative of some illnesses was registered for the first time in 1926 by Dr. William Koch, who studied mental illness in a child, and worked based on the hypothesis that after ingestion of chlorine dioxide in a solution of 3.5%, knowing as stabilized oxygen, oxygen was released and it will be transported to the brain improving the illness; however, the hypothesis was no successful proved [6]. Later in 1990, scientists Yu-Shiaw Chen y James M. Vaughn published a new work about the inactivation of human rotaviruses using chlorine dioxide in concentrations ranging from 0.05 to 0.2 mg/L [7]. The study of chlorine dioxide generates great interest in the scientific community and in July 2000 a patent denominate "Use of a chemically-stabilized chlorite matrix for the parenteral treatment of human immunodeficiency virus (HIV) infections was attributed to Dr.Friedrich W. Kihne [8], this patent does not have records of use or applications by laboratories or organizations

Nowadays, the use of chlorine dioxide has emerged due to the COVID-19 pandemic by which hundreds of thousands of people have died around the world. In the fight to look for the vaccines by the scientific community, many people opted for treatments not endorsed by World Health Organization (WHO). One of those treatments is the use of chlorine dioxide; however, at the same time, the intake of this substance has generated dilemma and concerning in the people.

2.1.1 Molecular Structure and Geometry

Chlorine dioxide is a molecule with one atom of chloride and two oxygen atoms linked through double bounds. The distance between Cl-O is 1.49 Å, while the angle O-Cl-O is 116.5° [9]. Chlorine dioxide possess a structure, which for many years was subject to the dilemma; however, currently, the best model that explains the structure (Figure 2.1) is one in which the unpaired electronic of the chlorine atom interacts in a resonance manner with the atoms of oxygen, thus giving great reactivity to the molecule through oxygen atoms [10].
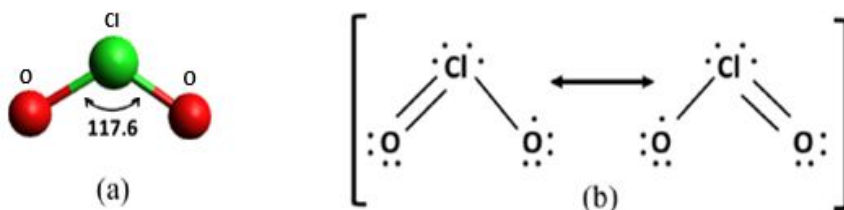
Figure 2.1: Lewis and molecular structure of chlorine dioxide

2.1.2 Chemistry of Dioxide Chloride

Chlorine dioxide is an unstable greenish gas, impossible to be compressed without causing an explosion, as consequence it must be generated *in situ* [11]. This molecule has a molecular weight of 67.46 g/mol, a boiling point of 11°C, its solubility in water is 3,000 mg/L at 25°C, and a specific gravity of 1,642 at 0°C (Table 2.1). In addition, chlorine dioxide is considered an oxidizing agent, that produces two consecutive reactions (Equations 2.3 and 2.4), in which oxidation potential in an aqueous solution decreases linearly by 0.062 V with each unit increase of pH [12].

$$ClO_2 + e^- \rightarrow ClO_2^- ; E_o^{25°C} = 1.15V \tag{2.3}$$

$$ClO_2^- + 4e^- + 2H_2O \rightarrow Cl^- + 4OH^- ; E_o^{25°C} = 0.78V \tag{2.4}$$
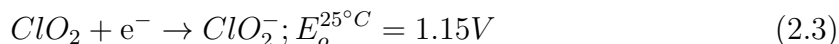
Property	Dioxide Chloride
Molecular Weight	67,452 g/mol
Chemical Formula	ClO_2
Color	reddish-yellow
Physical State	gas
Meting Point	-59°C
Boiling Point	11°C
Density	1.640 g/ml (0° C)
Solubility	3.01g/L at 25°C (water)

Table 2.1: Physical and Chemical Properties of Dioxide Chloride.
Taken from [11]

The experimental equation 2.5 can be used to evaluate the temperature dependence of the first redox potential of dioxide chloride [11].

$$E_0 = -5.367 + 0.0613T - 19.4X10^{-5}T^2 + 2X10^{-7}T^3 \qquad (2.5)$$

In comparison with other oxidizing substances, dioxide chloride is not as reactive as ozone or chloride. In table 2.2 we can show the oxidant strength of some common substances used as disinfectants.

Substance	Oxidant Potential	Oxidation capacity
ozone	2.07	$2e^-$
hydrogen peroxide	1.78	$2e^-$
dioxide chloride	0,95	$5e^-$

Table 2.2: Physical and Chemical Properties of Dioxide Chloride

Chlorine dioxide in aqueous solution gradually produce subproducts (Figure 2.2), between them chlorite $(ClO_2)^-$, and chlorate ions $(ClO_3)^-$, as the main decomposition products. For instance, if we take sodium chlorite as a precursor in hot, strongly alkaline solution, chlorine dioxide is not formed but chlorate ion is the principal product of the decomposition; in contrast, in acidic conditions, the products of the decomposition reaction are chlorate ion, chlorine dioxide, and chloride ion. [13, 14]. Otherwise, is reported that large excess of chlorine is needed to produce only chlorine dioxide and no chlorate [14].

In addition, ClO_2 has an odd number of electrons; as consequence, is considered a paramagnetic radical with an antibonding orbital. As a result, ClO_2 only reacts with five electrons being the maximum capacity 5 e^- in the reduction to chloride.
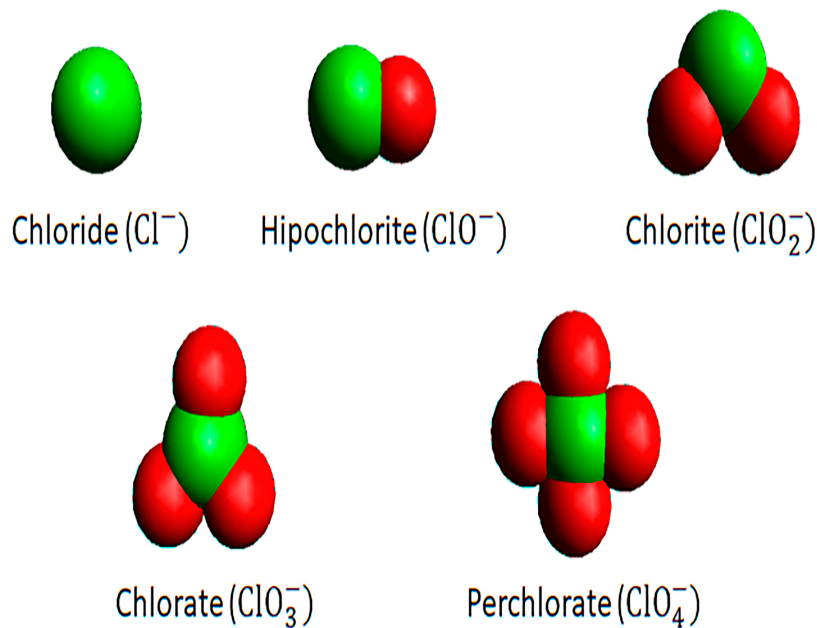
Figure 2.2: Molecular Structure of the main subproducts of dioxide chloride

2.1.3   Uses of Chlorine Dioxide

- **Water Treatment**.-One of the most common uses of chlorine dioxide is as a disinfectant in water treatment; due to its microbicidal effect. This substance shows an oxidant effect that in water can react with organic compounds as phenol and inorganic compounds as metal ions, this property improves the flavor and color of the water [5].

- **Food Industry**.-Chlorine dioxide can be used even in the food industry, due to the avoid the formation of trihalomethanes and compounds which can affect the health of the consumers, it is used in the disinfection of food, utensils, and machines food processors [15]. Moreover, ClO_2 can be used to control pathogenic and spoilage microorganisms and increase product shelf life [16].

- **As bleaching agent**.-Chlorine dioxide can eliminate lignin pigmentation. For this reason, it acts as a bleaching agent without altering its mechanical properties. In fact, ClO_2 acts not only with lignin but to a lesser degree on the hemicelluloses, with the formation of lignin and chloroligninic acids, in a selective way

without degrading the cellulose [17].

- **Medical**.- Chlorine dioxide is known as one of the most effective biocides against pathogens that can cause several diseases [5, 18]. For this reason, it is present in a series of products of personal hygiene as toothpaste and contact lens cleaner [19].

2.1.4 Chlorine dioxide and Human Health

When people drink chloride dioxide solution or water disinfected with this substance, it converts into chloride ions, those which are distributed in the organism. It is reported that around seventy-two hours after ingesting a single 100 mg/L dose, most of the chlorine dioxide was detected in the form of chloride ion (Cl_-), and the chloride-chlorite ratio (ClO_2) was 4 to 1 [20]. Once ingested, the compound is distributed throughout the body, but the highest concentrations are found in the blood, stomach, and small intestine.

Ecuadorian Association of Experts of integrative Medicine (AEMEMI) in Guayaquil, one of the worst COVID-affected regions in Ecuador, has used the treatment based on the administration of chlorine dioxide solution which they assure used in an appropriate and safe dilutions. This organization has reported a highly effective and low-cost alternative that can quickly contribute to the restoration of the individual's health infected with the human Coronavirus type 2, and it is assumed that it can promote the reduction of morbidity and mortality, as demonstrated with 104 COVID-19 patients [21]. Therefore, Dr. Andreas Ludwig Kalcker, who has been the promoter of the use of ClO_2 as a treatment against COVID-19, recommends a daily dose of 10 ml diluted in 1 L of water [22]. However, the idea of the consumption of chlorine dioxide is not acceptable by most of the scientific and medical community as well as the health organizations WHO.

Some studies about dioxide chloride have reported that its substance and its subproducts as chloride ions are strong oxidizers, that react quickly with water or moist body tissues, producing severe health problems.

2.1.5   Toxicity

Several studies about the toxicity of chlorine dioxide have been reported before [23–25]. The toxicity of this substance will depend on several factors like the administration route, either oral, respiratory, or dermal, the physical state, and of course of the concentration. There is no available information about the accurate value of the lowest-observed- adverse-effect-level (LOAEL) by inhalation in humans, but in rats was reported that at 1 ppm damage effects being expressed as alveolar vascular congestion, hemorrhagic alveoli, epithelial erosions, and inflammatory infiltrations of the bronchi [26, 27]. Therefore, based on the dead respiratory cases and accidental inhalation exposure on humans, the data indicate that airborne chlorine dioxide is a primary respiratory tract irritant [28].

On the other hand, oral exposure causes effects that include damage to the gastrointestinal tract, impairment of functioning normal thyroid gland, and mainly by the formation of methemoglobin [10, 29]. It was evidenced that the oxidative stress caused by ClO_2 in rat erythrocytes produced precipitation of hemoglobin as a consequence of the oxidative action of glutathione on the thiol groups of hemoglobin and inner membrane of the cell [30]. However, it has also been shown that chlorine dioxide induction of methemoglobinemia is due to ClO_2, ClO_2^-, but no ClO_3^- [31, 32]. By dermal exposure, although the information is limited, it is known that in mice solutions of chlorine dioxide at a concentration in a range of 9.714.4 mg/mL cause irritation [12].

2.2   Heme group as an active site in proteins

Heme is a prosthetic group present in some proteins called heme proteins like cytochrome P_{450}, peroxidases, hemoglobin, etc. Depending on the function, the heme group can be classified as heme-a, heme-b, heme-c, and heme-d, all structures have in common a macrocycle composed of a tetrapyrrole ring that usually harbors a ferrous atom, which is coordinated to the four nitrogen atoms [33]. In figure 2.7 we can see the different structures corresponding to the heme groups.

Inside of the heme family, heme-b is the most versatile, it acts as electron transport and plays an important role in the respiration process as well as photosynthesis; in addition, its prosthetic group serves for gas transport and sensing, and thus plays a role in signaling and transcription regulation [35].

The diversity of the biological functions of the heme proteins is directly related to the coordination state. Heme proteins usually have a five-coordinate heme center with
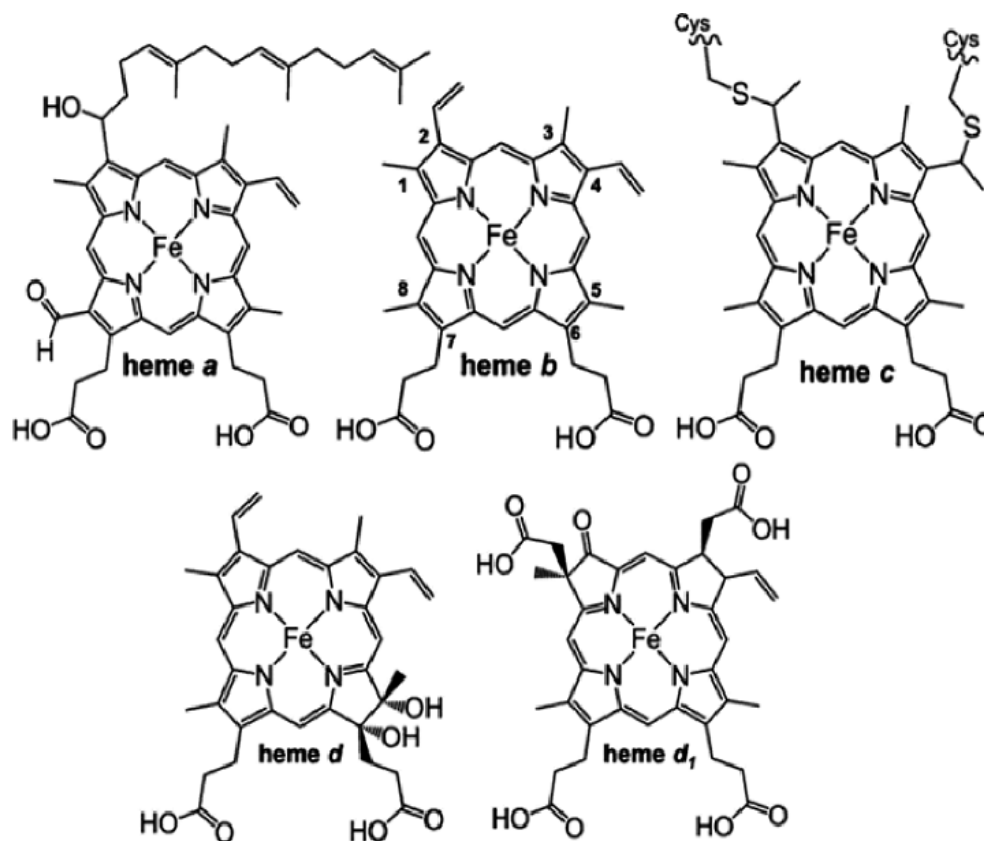
Figure 2.3: Structures of different heme groups. [34]

a vacant sixth ligation position [36]. In the case of the proteins, the heme group is connected by axial histidine and specifically to hemoglobin to an oxygen atom which is reversibly coordinated.

One of the main reasons for which nature chooses porphyrin ligands to do such diverse functions in biology is because the porphyrin macrocycle is conformationally flexible and can adopt a range of nonplanar structures [37]. The resting state of hemes in isolated proteins is planar in most cases; however, when the protein is bound to the substrate, the heme deviates significantly from planarity and the degree of non-planarity varies from one system to another [37, 38],but the types of heme distortions found in hemoproteins are energetically unfavorable, those are conserved in homologous proteins from different organisms, suggesting that heme distortion are important for their function [39].

2.2.1 Porphyrin Distortions

Tetrapyrrole molecules as porphyrins generally are highly symmetrical and planar [40]. However, a set of factors as bonding, electronic effects, cysteine thioether linkages between the porphyrin pyrrole groups and the polypeptide, bulky protein residues induce

the deformation of the planarity of the macrocycle [41]. The distortions are classified as: out of plane (saddling, ruffling, doming, X-waving, Y-waving, and propellering) , and in-plane (meso-stretching, N-pyrrole stretching, pyrrole translation, breathing, and pyrrole rotation) normal modes that relate to the structure of a distorted heme compared (Figure 2.8). Studies have suggested that heme distortion also controls the properties of heme, such as the UV–vis spectrum, the redox potential, and the ligand-binding affinity [42–44].
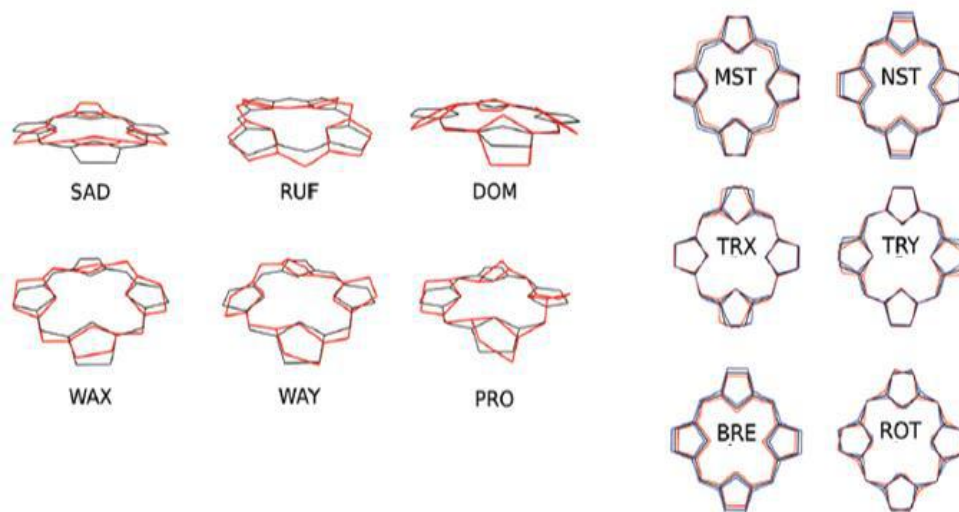
Figure 2.4: Heme distortions positive (red) and negative (blue). Left: out-of-plane distortions doming (dom), ruffling (ruf), saddling (sad), waving (wax, way) and propellering (pro). Right: in-plane distortions involving meso-stretching (mst), N-pyrrole stretching (nst), pyrrole translation (trx, try), breathing (bre), and pyrrole rotation (rot). Taken from [43].

2.3   Considerations about Iron

As known, in the heart of the porphyrin ring in heme proteins, an iron atom is located, which can exist in different oxidation states, and depending on it the functionality of the biomolecule such oxidation state can change. In the case of hemoglobin, the most common oxidation states are ferrous (Fe^{2+}) and ferric (Fe^{+3}) irons [45]; however, high oxidation states of iron as ferryl (Fe^{4+}), ferroyl (Fe^{5+} and Fe^{6+}) are present as key intermediates in the mechanisms of dioxygen activation in several proteins [46]. This section has a goal to know the main properties exhibit by the metal in its different states as well as to analyze the influence of the change of oxidation state in the protein perturbations.

2.3.1 Role of Iron in the Body

It is well known that the human body is composed of atoms that have been spatially arranged to produce the molecules and larger structures that sustain our lives. The largest elemental components of the body, by mass, are oxygen (65%), carbon (18%), hydrogen (10%), and nitrogen (3%) [47]. The other elements in the body, such as calcium, phosphorus, iron, and copper, are known to physiologists as mineral elements and trace elements. Those elements must be present in the body in the proper amounts, and those must be available to react with other elements to form critical molecules and participate in important chemical reactions.

The ability of metal ions to coordinate and then release ligands in some processes, and to oxidize or reduce in other processes makes them ideal for use in biological systems. The most common metal used in the body is iron, and it plays a central role in almost all living cells. For example, iron complexes are used in the transport of oxygen in the blood and tissues [48]. In the case of hemoglobin, iron can be coordinated to the porphyrin ring through the nitrogen as electron donor, which is in the plane, and as axial ligands nitrogen of the histidine distal and proximal. The number of coordination bonds that iron can form depends on the state of hemoglobin if it is a strain or relaxes [49].

Therefore, the oxidation state of the iron is crucial in the functionality of the hemoglobin, when in the environment there are oxidative agents, hemoglobinopathies can appeared as methemoglobinemia. It consists of the forms and "inactive" hemoglobin, by the oxidation of the ferrous iron to ferric iron. It means that methemoglobin is unable to be reversibly combined with oxygen, in addition, skews the oxygen dissociation curve in the sense of increased affinity for this and therefore hinders its transport from the blood to tissues [50].

2.3.2 Physical and Chemical Properties

Iron is a transition metal that belongs to group VIII of the periodic table, which has the symbol Fe and atomic number 26. This metal has four oxidation states, +2 and +3, +4 and +6 states, the last is known but less common. Compounds of iron in the +2 state are designated ferrous and contain the pale green Fe^{2+} ion; while compounds of Fe^{+3} state are called ferric and present a characteristic yellow to orange color depending on the extent of hydrolysis or complex ions.

Depending on the oxidation state, physical and chemical properties will be different. Ferrous iron has an ionic radius of 0,76 Å and ferric 0,64 Å, and the standard redox potential is $0,77$V as shown in the equation 2.6.

$$Fe_{aq}^{+3} + e^- \rightarrow Fe_{aq}^{+2} \qquad + 0,77V \qquad (2.6)$$
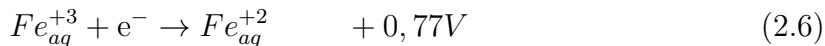
From a point of view of the acid-base of Pearson, a hard acid is a species that possess a positive charge and that can accept electron pairs, they are characterized by being small cations, of low electronegativity, high charge, and low polarizability, while a soft acid is characterized by possessing low charge density, to be large in size and easily polarized, so based on Pearson theory, the ferric ion is hard acid and ferrous ions are considered a borderline acid.

2.3.3   Structural Analysis

Iron in hemoglobin can form five and six bounds depending on if it is coordinated to substrate or not, in this case, dioxygen. In the plane ferrous iron is bounded to the four nitrogen atoms corresponding to the pyrrole ring and the two axial ligands corresponding to the nitrogen of the histidine and oxygen as shown in figure 2.5.
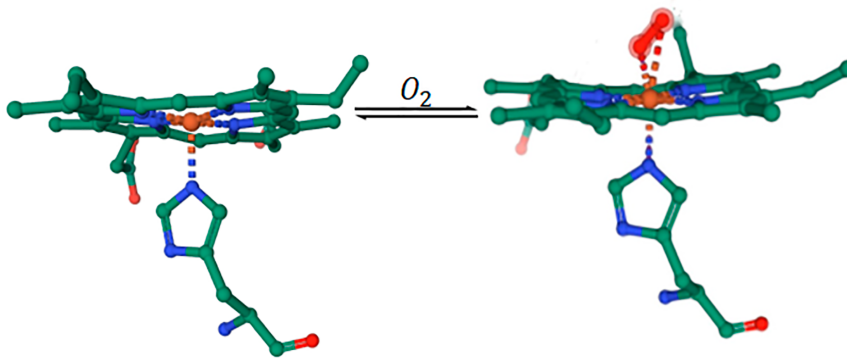
Figure 2.5: Structures of heme groups in their oxy and deoxy forms

On the other hand, the ferrous complex can show deformations in the octahedral geometry, explained by the Jahn Teller effect. The theorem postulate that non-linear molecules in the basal electronic degenerate state suffer a geometrical distortion, and the effect of the distortion decrease the energy of the molecule [51]. In the case of the octahedral complexes when the axial ligands move away from the central ion suffer a tetragonal distortion or elongation and contrary if the axial ligands get closer to the metal center the complex suffers a tetragonal contraction [52]. The Jahn Teller effect is more visible in metals with electronic configuration d^7, d^9 low spin and d^4, d^9 high

spin. In the case of heme group Fe^{+2} that possesses a d^6 sell valance of has a weak distortion in high spin and no distortion in low spin form; however, the opposite effect is evidenced in complex with Fe^{+3} as shown in table 2.3.

Sell valance	d^1	d^2	d^3	d^4	d^5	d^6	d^7	d^8	d^9	d^{10}
low spin	w	w		s		w	w		s	
high spin	w	w		w	w		s		s	

Table 2.3: Strenght of the Jahn Teller effect according to the spin state, letter w is for weak and s for strong. Take from [53].

2.4   Hemoglobin

Several studies have been carried on in order to understand one of the most important proteins, hemoglobin (Hb). Those began in the early 1800s when hemoglobin was found to be a major component of mammalian blood cells containing iron [54].

Hemoglobin is a globular protein conformed by two alpha and two beta chains, each one binds one heme, the prosthetic group (Figure 2.6). Moreover, the alpha chain is in contact with the beta chain, but less interaction between chains of the same type [50]. It is present in high concentrations in red blood cells, and its main biological functions are the transport of O_2 to the peripheral tissues and the transport of CO_2 and protons H^+ from the peripheral tissues to the lungs [50]. According to World Health Organization, hemoglobin normal level ranges between 120 and 130 gL for adults and abnormal Hb concentration leads to Anaemia, leukemia, and thalassemia
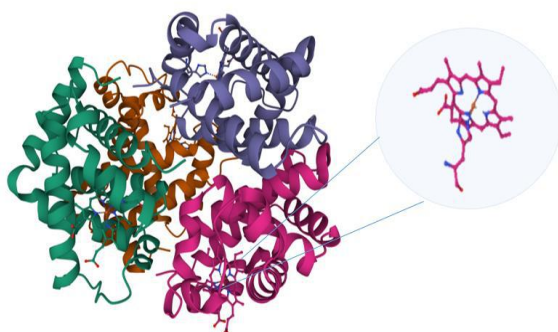
Figure 2.6: Structures of deoxyhemoglobin code:1a3n PDB

Hemoglobin can adopt two conformations tense or relaxed, so if hemoglobin is in the deoxygenated form, it adopts tense confirmation, while if it is in oxygenated forms,

it prefers relaxed conformation (Figure 2.7). The conformational change associated with the transition from tense to relax mainly affects the relative position of the dimers alpha and beta rather than the interactions between those subunits within a dimer [55].
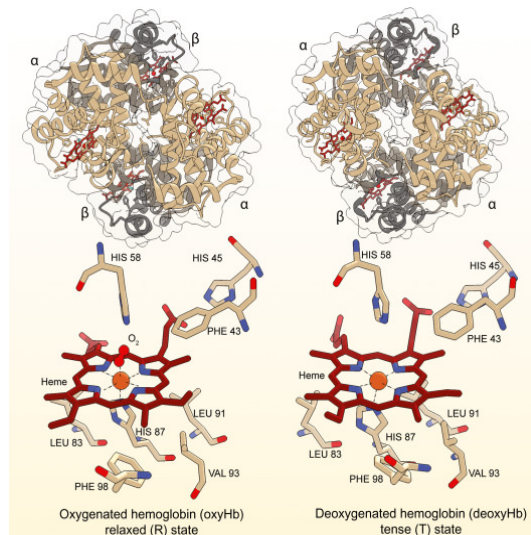
Figure 2.7: Tense and relax (T → R) conformational transitions of hemoglobin. Taken from [56]

2.4.1   Methemoglobin

Methemoglobin is known as ferri-hemoglobin too, it is a dysfunctional form of hemoglobin that is incapable of transporting oxygen because of the oxidation of ferrous ion to the ferric form [57]. It is worth noting that a small amount of methemoglobin is always being formed in the process of oxygenation-deoxygenation [58], but it is reduced by enzymatic processes within the red blood cells, one of the most remarkable NAD reductase methemoglobin systems (Figure 2.8). Depending on the origin methemoglobinemia can be classified into two groups, Acquired, and Congenital types.

- **Acquired Methemoglobinemia:** it is a consequence of the exposure to oxidizing agents like aniline dyes, antipyrine, arsine, benzene derivatives, chlorates, chlorobenzene, chloroquine, etc. Those exogenous agents can accelerate the production of MetHb or inhibit the protective enzymatic systems that normally maintain MetHb at low levels [60, 61].

- **Hereditary Methemoglobinemia:** it is due to a genetic defect in red blood cell metabolism or hemoglobin structure or by the absence of an enzyme needed in the body's natural reducing systems (e.g., Cytochrome-b5/b5 reductase deficiency) [62].
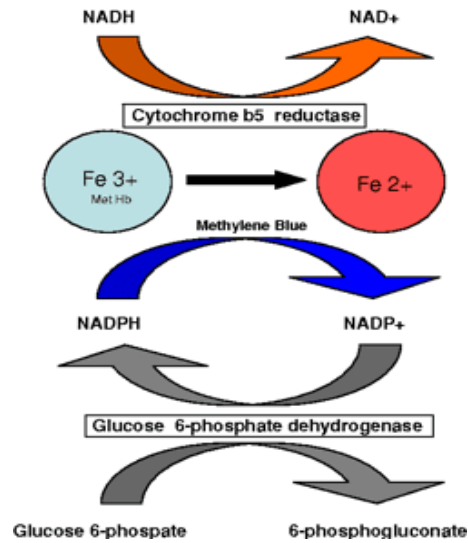
Figure 2.8: Mechanism of action of methemoglobin. Taken from [59]

Methemoglobin levels of 30˘45% result in headache, fatigue, tachycardia, weakness, and dizziness, while levels above 60% result in cardiac arrhythmia, dyspnea, seizures, and coma. Death typically occurs at MetHb levels > 70% [63].

2.5 Catalase-Peroxidase (CAT-2) from *Neurospora crassa*

Catalase-Peroxidase (CAT-2) is an enzyme isolated from the fungi Neurospora crassa. This type of enzyme has an important biological function, due to can act as a protected agent against reactive oxygen species (ROS) damage, and as its name suggests it is a bifunctional protein. CAT-2 is a homodimer with a molecular weight of 177 kDa (Figure 2.9), which possesses a heme-b group as an active site with the metal center in its oxidized form (Fe^+3). The heme-b group is coordinated to the axial histidine forming a pentacoordinate structure. In addition to the active site, an important prosthetic group conforms by WYM is located to the proximal end of the heme cavity. The change or substitution of any of those amino acids results in the diminution of the catalytic activity of the enzyme [64].

Catalase-Peroxidase has been widely studied by its antioxidant and immunogenic properties; however, its relevance in this study lies in its use as heme-**b** source, which experimental details are addressed in the following section.
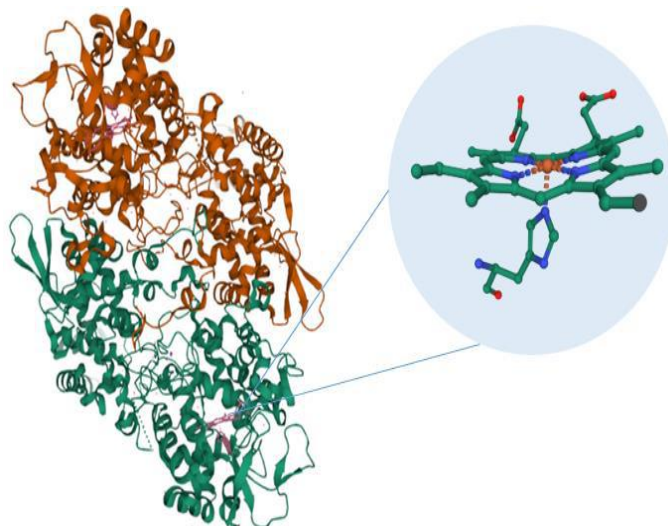
Figure 2.9: Tridimensional structure of Cat2 enzyme. Taken from PDB
5WHQ

2.6   Computational Background

Computational chemistry is a field of chemistry, which mainly aims at modeling and predicting the properties of a molecular system [65]. In this sense, computational chemistry becomes a powerful tool complementary to experimental chemistry that offers rewarding information in the understanding of the behavior of the system. Among the most common methods used are molecular mechanics, ab initio, semi-empirical, and density functional theory DFT.

2.6.1   Density Functional Theory

Density functional theory is based on the two Hohenberg–Kohn theorems, which state that the ground-state properties of an atom or molecule are determined by its electron density function and that a trial electron density must give energy greater than or equal to the true energy [66]. DFT formulate the problem of the quantum mechanics of the electronic structure in terms of an observable quantity, the density electronic, instead of polyelectronics wave function [67].

Density functional theory is a useful tool to investigate the structure and properties of complicated organic and inorganic molecules, such as coordination compounds, due to the high accuracy that can be achieved at a relatively low computational cost [68]. Because DFT works partitioning the electronic energy in components that are computed individually, it is a method profitable in the study of metal-organic molecules as the complexes analyzed in this search. The components of the electronic energy of the

DFT functionals are kinetic, nucleus-electron interaction, electron-electron interaction, and Coulomb repulsion [69].

2.6.2 Definition of B3LYP

B3LYP is a hybrid functional of DFT, which has shown successful prediction of a wide range of molecular properties. B3LYP becomes the most popular and most widely used functionally. This amazing success was fueled by the surprisingly good performance B3LYP and related functionals are demonstrated in many chemical applications, including such difficult areas as open-shell transition-metal chemistry [70].

2.6.3 Mulliken Population Analysis

Mulliken population analysis is one of the most widely used schemes for electronic density understanding. Population Analysis is a mathematical way of partitioning a wave function of electron density into charges on the nuclei [71]. The assumption by Mulliken Population works is the half-and-half partition of the overlap populations, into equal charges in orbitals [72]. Generally, oxidation states (OS) are assigned with an integer number of electrons to the atoms according to a set of rules. However, in compounds that involved non-innocent ligands, intermediates, or transition states of reactions the formal OS could be ambiguous and for this reason, computational approaches are used [73].

2.6.4 Software Used

Nowadays, the use of some computational programs is essential in theoretical chemistry. The two most important programs used in this study are Avogadro and Orca. Avogadro is free software that lets us visualize molecules or draw them; in addition, it is a useful tool to know the structural and electronic parameters of the molecule as well as its optimization geometry. Moreover, Avogadro can be used not only to prepare input files for a range of computational chemistry software but also to visualize output files from them [74]. On the other hand, Orca is a software with a variety of methods including a wide range of implemented theoretical methods, robustness, efficiency, and focus on transition metals, optimization of geometry, and spectroscopic properties [75]. Those features become Orca in one of the most widely used electronic structure codes in the computational chemistry community [76].

Chapter 3

Methodology

3.1   Computational Analysis

3.1.1   Optimization Geometry of iron complexes

In order to understand the interactions and the mechanism of the redox reaction between the chlorine dioxide and heme-b group, optimization geometry calculation was achieved. To aboard this study, five iron complexes were optimized, which are shown in table 3.1.
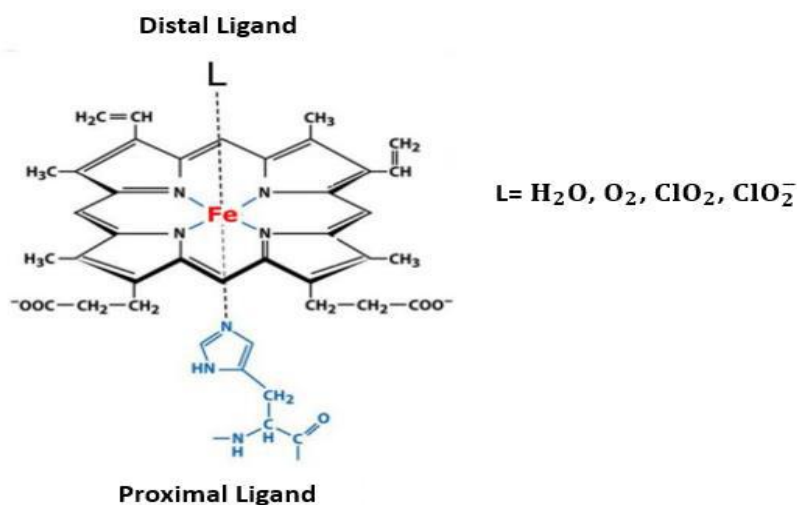
Figure 3.1: Scheme of the general heme complex with distal ligands studied

The iron complexes were studied with four different distal ligands as we can observe in figure 3.1. The initial structures were the ligands, water, oxygen, chlorine dioxide, and chlorine ion. Then L0 complex was taken from Protein Data Bank PDB code 1a3n [77] and optimized too.

Because L3 and L4 complexes can interact with metal center either by Cl^- or O_2, the two forms were optimized to elucidate which are the conformation more suitable

Name	Chemical Formula	Code
histidineporphiryniron (II)	$[\text{Fe}(\text{ppIX})(\text{his})]^+$	L0
ion aquahistidineporphiryniron (II)	$[\text{Fe}(\text{ppIX})(\text{his})(\text{H}_2O)]^+$	L1
ion histidineoxygenporphiryniron (II)	$[\text{Fe}(\text{ppIX})(\text{his})(\text{O}_2)]^+$	L2
ion chlorinedioxidehistidineporphiryniron (II)	$[\text{Fe}(\text{ppIX})(\text{his})(\text{ClO}_2)]^+$	L3
chlorinehistidineporphyriniron (II)	$[\text{Fe}(\text{ppIX})(\text{his})(\text{ClO}_2)]$	L4

Table 3.1: Study complexes

energetically which are $L3$ and $L4$ respectively. Moreover, the L0 complex was computed in their high and low spin according to the magnetic properties reported of the hemoglobin, either in oxygen or deoxygen forms, which are labeled $L0$ and $L0$ respectively.

The optimization was calculated using ORCA software and the general input for it is shown in figure 3.2.

```
# avogadro generated ORCA input file
# Basic Mode
# Heme6_R
! B3LYP D3BJ OPT def2-SVP PAL4

* xyz 1 5
    N         9.87852        28.36322        -3.60568
    C        10.37566        29.26225        -4.63374
    C        11.20163        28.49193        -5.65703
```

Figure 3.2: Input for optimization geometry

Once to get the optimization of the complex L0, different ligands were coordinated forming an octahedral geometry. The study of the iron complex was probed with four different axial ligands between them: oxygen, water, chlorine dioxide, and chloride ion. Those ligands were chosen in order to simulate the physiological conditions.

In the case of the complex L0 the total charge of the molecule is $+1$ conferred by the histidine amino acid, and multiplicity $S = 5$, while the complexes L1, L2, and L3 were computed with a total charge of $+1$ and multiplicity $S = 1$. The last complex L4 was computed with neutral total charge and multiplicity $S = 1$.

3.1.2   Mulliken Population Analysis

The influence of the ligands in the electronic charge of the complexes (Figure 3.3) was estimated using the Mulliken Population Analysis obtained from the previous geometry optimization. To determine the value of the oxidation state, the direct atom ligand to

the iron metal center was considered. The sum of the electronic contributions to the metal center gives as an approximation of the oxidation state of the iron.

Figure 3.3: Output for Mulliken Population Analysis

3.1.3   Structural Properties

Through the optimization geometry, some important parameters as bond length and angles were measured with Avogadro. Those parameters were analyzed to identify the molecular geometry either square base pyramid and octahedral, and the distortions that complexes could present. To carry out the measurements, all complexes were reduced to the first coordination sphere, which implies that only the first direct atom coordinates to the metal center (Figure 3.4).
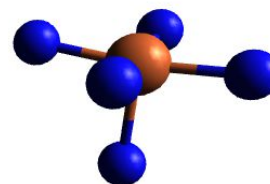
Figure 3.4: Scheme of the length bonds of the first coordination sphere measured in Avogadro

3.1.4   Electronic Properties

Some important electronic properties were calculated to understand the reactivity of the complexes. Those properties are directly related to the boundary orbitals, HOMO

and LUMO. Between the electronic properties is the bandgap energy (E_G) defined as the equation 3.1

$$E_G = E_{HOMO} - E_{LUMO} \tag{3.1}$$

The ionization potential (I), which is the measurement of the energy required to separate an electron of a molecule, was computed through equation 3.2, shown below.

$$I = -E_{HOMO} \tag{3.2}$$

Then, the electronic affinity (EA) was determined according to equation 3.3

$$EA = -E_{LUMO} \tag{3.3}$$

Another, electronic parameter studied was the chemical potential (μ) (Equation3.4) with the aim to analyze the electron flow from the less electronegative regions to the highest.

$$\mu = \frac{E_{HOMO} - E_{LUMO}}{2} \tag{3.4}$$

On the other hand, chemical hardness (η) was calculated as equation 3.5, let us estimate because it gives an idea of the resistance that the complexes have faced to the change of the electronic distribution.

$$\eta = \frac{E_{LUMO} - E_{HOMO}}{2} \tag{3.5}$$

3.2   Experimental Analysis

The experimental methodology to evaluate the reactivity between the model enzyme CAT-2 and chlorine dioxide follows a set of steps that begins with the isolation and purification of CAT-2, the protein was obtained by transformation of E.coli M15/pREP4 strain that contains pQC2-3D plasmid, in which cat2 gen was introduced and then the overexpressed protein was purified. After the purification, electrophoresis was carried out, followed by quantification of CAT-2, and finally the treatment of it with chlorine dioxide, which result was recorded through electronic spectroscopy. Each one of the steps mentioned is listed and detailed below.
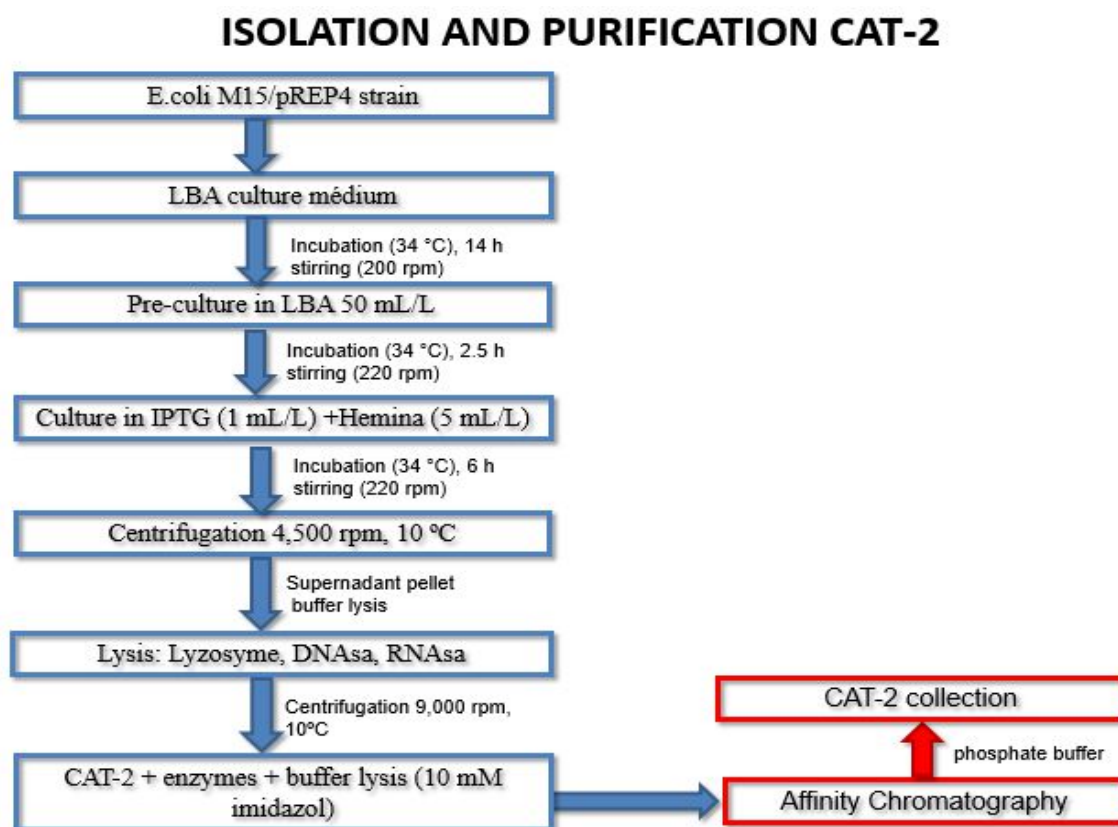
Figure 3.5: Scheme of the isolation and purification steps of CAT-2 enzyme. Taken from [78]

3.2.1   Isolation and Purification of CAT-2 enzyme

The experimental section begins with isolation and purification of CAT-2 enzyme, all processes follow a set of steps summarized in figure 3.5.

The isolation of the CAT-2 enzyme required the pre-cultured preparation of E.coli M15/pREP4 strain incubating a single colony of E. coli cells in 50 mL of liquid LBA culture medium at $34°C$ and 220 rpm during 14h. This step was repeated but this time in a ratio of 50mL/L of precultured per liter of liquid LBA culture media at $34°C$ and 220 rpm but only during 2.5h. Once the culture has been obtained, it was induced with IPTG (1mL/L) and hemin (5mL/L) at $34°C$ and 220 rpm during 6h. Then, the cells culture was collected by centrifugation at 4500 rpm and $10°C$. After that, resuspension of the pellets collected was carried out in 20 mL of lysis buffer (50mM NaH2PO4, 300mM NaCl, 10mM imidazole; pH=8.0) in order to induce cellular disruption. Moreover, due to the viscosity of the cell extract, second lysis was made using a solution of lysozyme (100mg/mL) in aliquots of 30 mL $4°C$, DNase, and RNase 5µL of each one at $37°C$ until viscosity disappears. Finally, protein extract was collected in fractions of 1mL after centrifugation at $10°C$ and 9000 rpm.

The purification of the protein was through affinity chromatography to nickel, using a column of 15cm large and 1,5cm of diameter which was loaded with Ni-NTA resin and protein. Then, 25mL of lysis buffer, 100mL of wash buffer (50mM Na_2PO4, 300 mM NaCl, 20 mM Imidazole, pH:8) were used to wash the resin. The interaction of the CAT-2 with the resin through the nitrogen of His (Base Lewis) with Ni^+2 (Acid Lewis) let that the enzyme remain retained in the column. Then to guarantee the total elution of the CAT-2 40mL of elution buffer (50mM Na2PO4, 300mM NaCl, 250mM Imidazole, pH:8) was used and then is observed the protein by its red characteristic color conferred by the Fe^{+3}. The last step was the collection of CAT-2 fractions in a tube containing phosphate buffer (Na/K 50mM, pH:7.8).

3.2.2   Electrophoresis

Once collected CAT-2 enzyme, the next step is to corroborate the presence of the CAT-2 enzyme and at the same time evaluate the efficiency of the separation of other proteins that may be present in the samples. For that, sodium dodecyl sulfate-polyacrylamide gel electrophoresis (SDS-PAGE) was used with the aim to Mini- PROTEAN Cell equipment. The electrophoresis was made using 8% polyacrylamide gel and running buffer (3.3 g of trizma base, 14,4g of glycine, 1L of distilled water, and 1g of SDS, pH: 8.3) during 50 min at 150v. Once to finish the electrophoresis the gel was colored with Coomassie Brilliant Blue.

3.2.3   Quantification of the CAT-2 enzyme in the cell extracts

The quantification of the enzyme in the cell extract was achieved following the Bradford method. For this, a standard dissolution of BSA (0.5 mg/mL) was prepared in 0, 2.5, 4, 6, 8, 10, 16, 20, and 30 mg/mL; therefore, 100µL of protein samples was taken in Eppendorf flask, and then, to each one 1mL of Bradford reagent was added and stirred. Finally, the absorbance was measured at 595 nm.

3.2.4   Reaction of CAT-2 with ClO$_2$

In order to evaluate the reactivity of CAT-2 with ClO_2, 1 mL of 70 μM of pure CAT-2 was treated with 1 mL of commercial chlorine dioxide solution with a final concentration of 70 μM reaching then a stoichiometric mixture of the enzyme and chlorine dioxide. Then the solution is loaded in a UV quartz cube (1 cm optical path) to record the electronic spectrum. Then, in order to identify if chlorine dioxide and a heme-b group

of CAT-2 interact through a redox reaction, the spectrum CAT2-ClO_2 was compared with the spectrum obtained by the reduction of CAT-2 with dithionite.

Chapter 4

Results and Discussion

4.1 Computational Results

4.1.1 Optimization geometry of L0 complex

The optimization geometry of the complex L0 shows that, in absence of the sixth ligand heme-b exhibit paramagnetic properties which are in agreement with the report in the literature [4]. In table 4.1, we can see that the final energy values are close; however, $[Fe(ppIX)(his)]^+$ is more stable in the high spin arrangement. The complex L0, that is the complex with multiplicity $S = 1$, differs in $\Delta E = 43.417E_h$ from $L0$, that is the complex with multiplicity $S = 5$, so it means that the complex with magnetic properties is less stable than which with paramagnetic properties. It is in agreement with the literature due to the physiological conditions the heme-b group presents paramagnetic properties. For this reason, the $L0$ complex was chosen for the following analysis with different ligands.
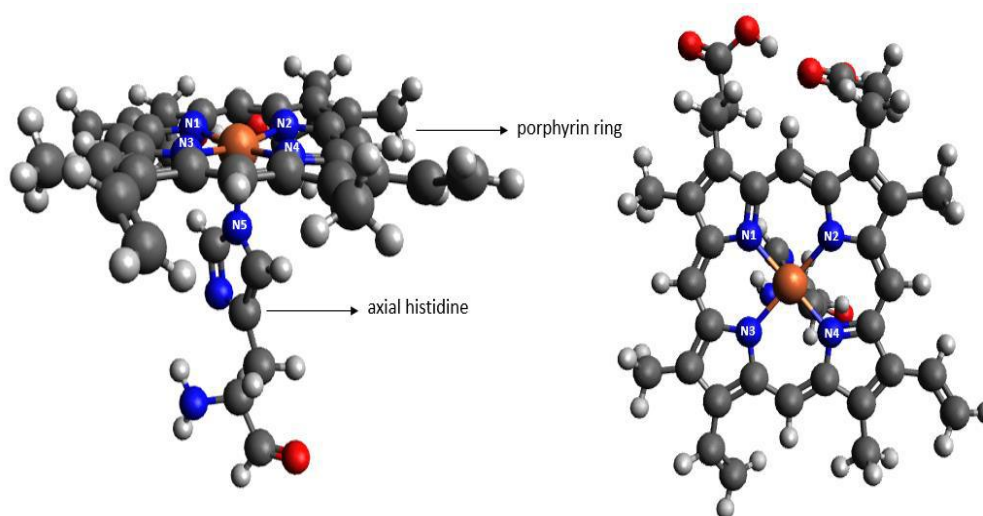
Figure 4.1: Different point of view of L0 complex

Code Complex	Spin	Energy (Eh)	Energy (KJ/mol)
L0	1	-3568.302	0
L0'	5	-3568.286	-43.417

Table 4.1: The energy of the L0 and L0' complexes

In figure 4.1 we can see the structure of the L0 complex, which has square pyramidal geometry. Here, the porphyrin ring is located in the plane while histidine is coordinated in an axial position.

4.1.2   Optimization Geometry of L1, L2 complex

Following with the atoms numeration of the complex L0, the next iron complex was optimized taken as base L0 complex. In figure 4.2 we can observe the two structures corresponding to the octahedral complex which ligands are: H_2O and O_2. An evident conformational change with respect to the L0 complex is observed, it is known as porphyrin deformations. In the case of the L1 and L2 complexes, present saddling *(sad)* out of plane distortion.
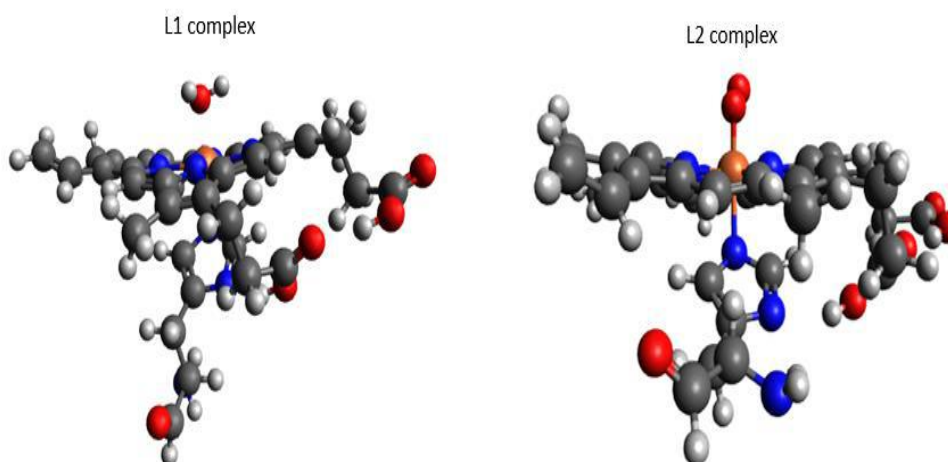
Figure 4.2: Optimized structure of L1 and L2 complexes

As we can see in table 4.2 the complex L1 has an energy major than L2 complex. In addition, the geometry change, L1 complex present a square bypiramidal while L2 complex an octahedral geometry.

Code Complex	Energy (Eh)	Energy (KJ/mol)
L1	-3644.6323	-9568982.7978
L2	-3718.4028	-9762667.1704

Table 4.2: The energy of the L1 and L2 complex

4.1.3 Optimization Geometry of L3, L3' complexes

The complexes L3 and L3' which correspond to the heme group with chlorine dioxide as a ligand (Figure 4.3), show that energetically L3' is more stable than L3 (Table 4.4) with an energy difference of ($\Delta E_h = 0.0297$). This is not a larger value between them; however, there is a significant difference in energy of ($\Delta E_h = 459.9668$) with respect to oxygen as axial ligand. It means that there is a major affinity to the complex by coordinating with chlorine dioxide than an oxygen molecule.
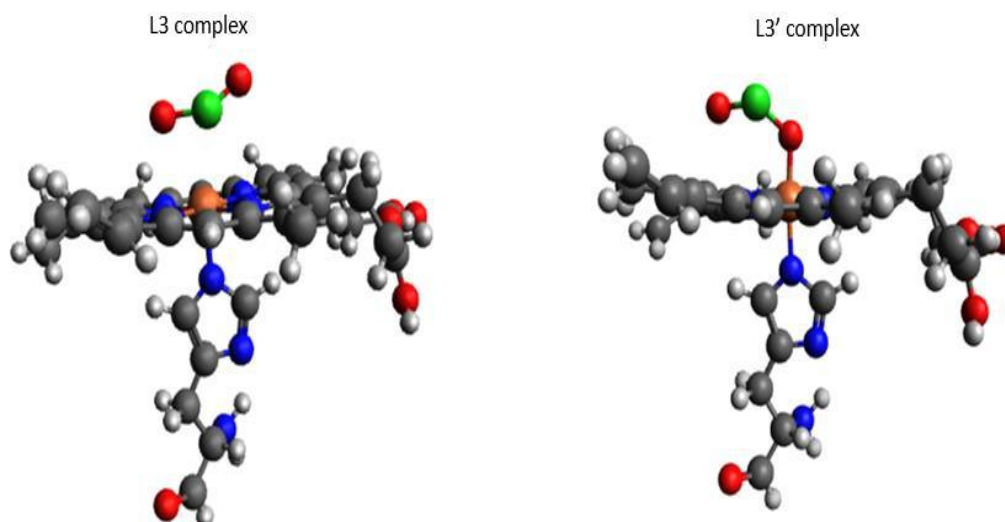
Figure 4.3: Optimized structure of L3 and L3' complexes

The major stability of those complexes in comparison with the L2 complex, give us an idea of the ingestion of chlorine dioxide solution can form those complex that by the major stability of the oxygen coordinate ClO_2, this result supports the idea that chlorine dioxide could cause an alteration in the heme-b group function due it prefers the conformation with chlorine dioxide as ligand.

Code Complex	Energy (Eh)	Energy (KJ/mol)
L3	-4178.3399	-78.1
L3'	-4178.3696	0

Table 4.3: The energy of the L3 and L3' complex

4.1.4   Optimization Geometry of L4, L4' complexes

The last two structures analyzed L4 and L4' corresponds to the complex coordinate to the chloride anion (Figure 4.4). To elucidate if ligands bind or not to the metal center and if it happens by oxygen or chlorine atom, final point energy was taken as the main parameter to know the stability of those complexes, which is present in table 4.4.
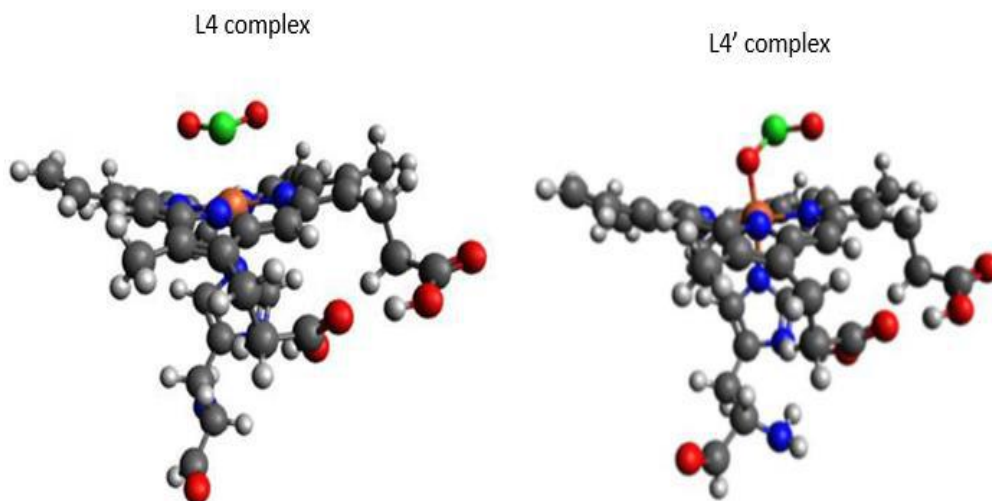
Figure 4.4: Optimized structure of L4 and L4' complexes

As we can see, although the energy difference between L4 and L4' is minimum ($\Delta E_h = 0.2972$) the most stable conformation is the complex coordinate to an oxygen atom.

Code Complex	Energy (Eh)	Energy (KJ/mol)
L4	-4178.5695	-78.1
L4'	-4178.5992	0

Table 4.4: The energy of the L4 and L4' complex

The optimization geometry of the complexes shows that of the four ligands ClO_2^- is the most stable followed by ClO_2. This behavior can be observed in figure 4.5 which shows how energy decrease according to the interaction with the ligands.

4.1.5   Mulliken Population Analysis

The calculation of atomic charges plays an important role in terms to describe the electron distribution of a compound as broadly as possible. The total atomic charge
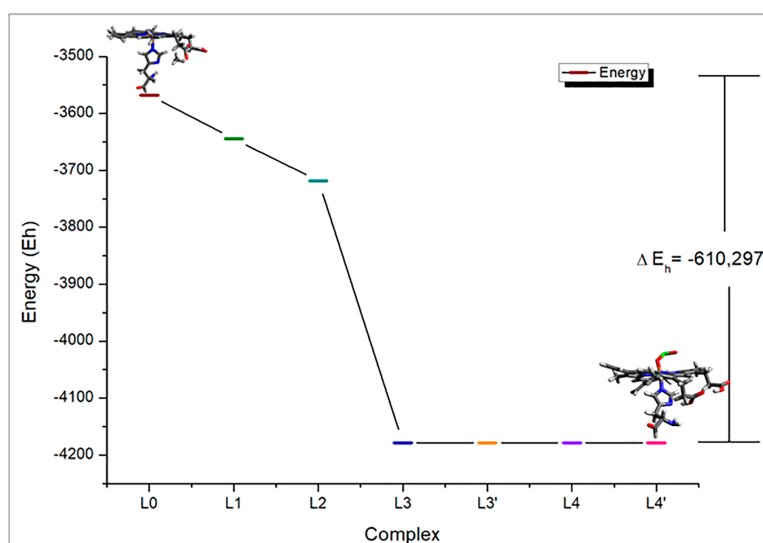
Figure 4.5: Energy profile of the complexes studied

values of the study complexes, obtained by Mulliken Population of the optimization geometry are listed in the table. The Mulliken Analysis was considered only for the complex L1, L2, L3' and L4', which are the most stables.

Complex	Atom	Mulliken charges
L0	Fe	0.799625
L1	Fe	0.542759
L2	Fe	0.528908
L3'	Fe	0.598789
L4'	Fe	0.453403

Table 4.5: Mulliken charge of an iron atom corresponding to the optimized complexes

The Mulliken charge values show how ligands influence the iron electronic density. In absence of the ligand, iron has a major positive electronic density around itself; nevertheless, when water and oxygen interact with the complex, those by the action of the oxygen atom reduce the positive charge, due to the major electron affinity affected by the second oxygen atom in the case of the L2 complex, the electronic charge here is less positive that with water in L1. In addition, the same effect is observed with chloride dioxide L3', and chlorite ion L4'. In those cases, when the ligands are coordinated through an oxygen atom to iron the effect of the loss of the electronic charge is more than the effect produced by the interaction through chloride atom.

Therefore, Mulliken charges can give us an idea of the oxidation state of the iron center. Figure 4.6 corresponds to the structure of the complexes only with the direct atoms binding to the metal center. Those atoms are the most electronegative, and they imply their influence on the oxidation state of the iron. In tables 4.5 and 4.6 we can appreciate the electronic charge change by the influence of the ligands and the Mulliken charge of the first coordination sphere respectively.

Atom	L1	L2	L3'	L4'
N1	-0.2209	-0.2212	-0.1936	-0.2120
N2	-0.2687	-0.2300	-0.2390	-0.2353
N3	-0.2496	-0.2119	-0.2557	-0.1979
N4	-0.2634	-0.2091	-0.2488	-0.2249
N5	-0.2396	-0.2068	-0.2723	-0.2154
O1	0.1733	-0.0833	-0.4456	0.4221
O2	NA	-0.0569	-0.4227	0.4456
H1	0.2045	NA	NA	NA
H2	0.2023	NA	NA	NA
Cl	NA	NA	0.6727	0.6736
Fe	0.5427	0.5289	0.5987	0.5218
Total	-0,4661	-0,6906	-0,853742	-0,7575

Table 4.6: Mulliken charge of the first coordination sphere of iron complexes. The use of abbreviation NA means no apply

The sum of the absolute value of the most influence atoms in the electronic density of iron gives an idea of the total electronic charge of it which corresponds to 2.36, 1.75, 3.35, and 3.22 for $L1$, $L2$, $L3'$, and $L4'$. The electronic charge values expected are $+2$ to $L1$ and $L2$ complex and $+3$ for $L3'$ and $L4'$. As we can see the Mulliken charge is near to the expected values; however, it is only an approach to know how the atoms directly binding to the iron influence the change of its electronic density of it.

4.1.6　Structural Properties

To effect, the understanding of the length of the bonds, the direct atoms linked to the iron metal center was labeled. Tables 4.8 and 4.9 presents the main bond length and angles of the L1, L2, L3, L3', L4 and L4'complexes.

The complex L1 does not form a new bond with a water molecule, so it complex keeps a square base pyramid geometry, but a distortion in this geometry is evident. In the case of the L2 complex, it forms a sixth bound with oxygen molecule; as a result, an octahedral geometry is obtained with bond and angles near to 2Å and 90°.
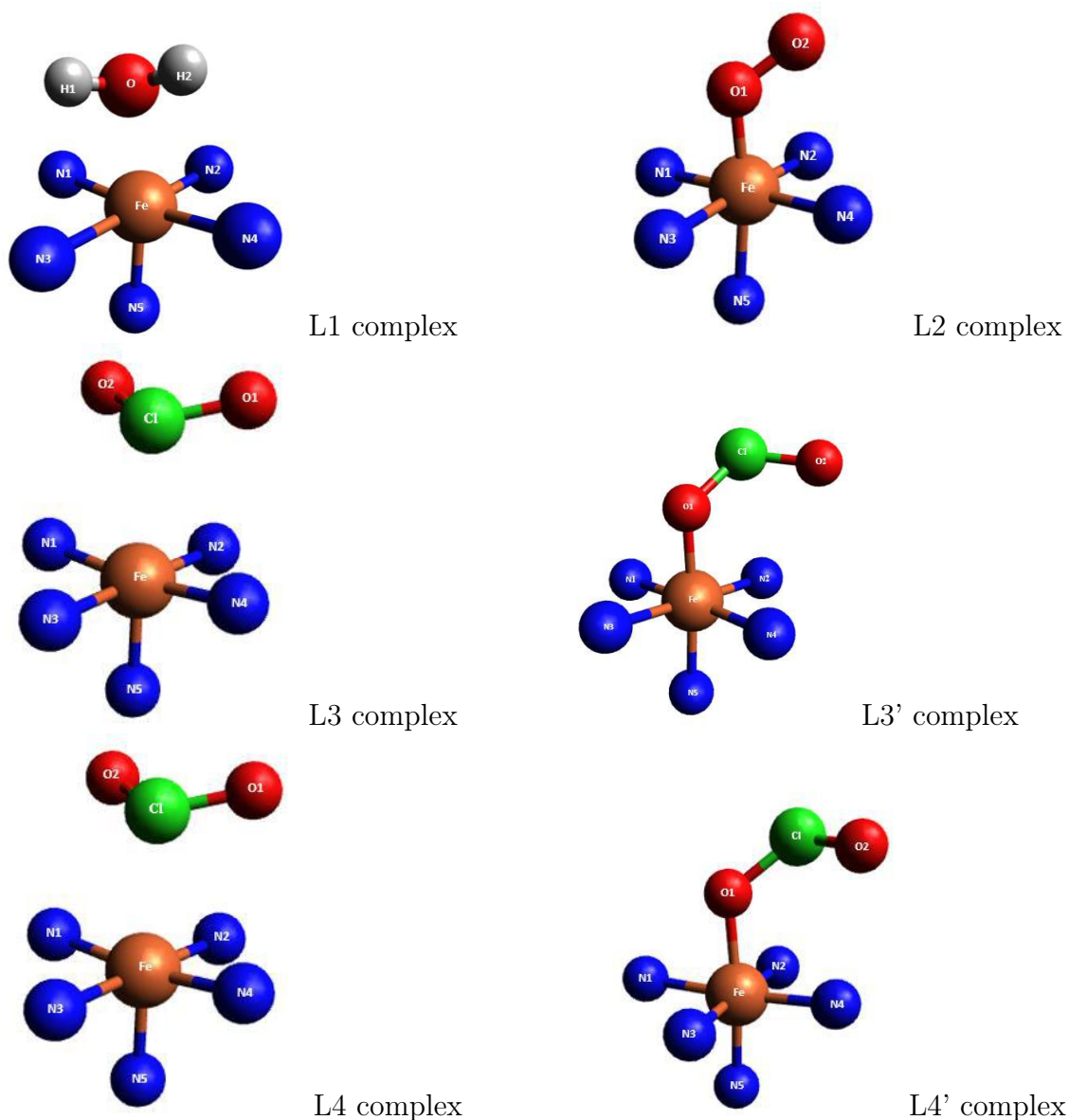
Figure 4.6: Structure of reduce firth coordination sphere of the L1, L2,
L3, L3', L4 and L4'

Atoms	L1	L2	L3	L3'	L4	L4'
Fe-N1	1.9899	2.0399	1.9734	1.9906	1.9684	1.9856
Fe-N2	2.0069	2.0725	2.0558	2.0351	1.9607	1.9400
Fe-N3	2.0056	1.9391	1.9560	1.9844	2.0148	2.0432
Fe-N4	2.0003	2.0086	1.9658	2.0007	2.0006	2.0355
Fe-N5	2.1198	1.9451	2.0705	2.0962	1.9416	1.9673
Fe-O1	NA	1,7633	NA	1.7632	NA	1.8990

Table 4.7: Bond length distance (Å) of the first coordination sphere of
of iron complexes

Atoms	L1	L2	L3	L3'	L4	L4'
N1FeN5	93.3441	94.9584	98.7696	87.6148	95.1750	93.8720
N2FeN5	96.1670	81.7313	96.9920	90.8213	86.0546	86.4574
N3FeN5	95.5310	99.9209	84.4947	89.9170	96.2370	88.4852
N4FeN5	94.5442	92.8845	81.1290	88.3448	92.5902	90.0880
N1FeN2	89.4441	89.5971	84.9717	90.6076	90.3144	91.2296
N2FeN4	89.6426	89.5971	95.9701	89.2547	89.3692	90.0245
N3FeN4	89.6166	91.2649	97.4014	90.9362	90.6306	89.7324
N3FeN1	89.6902	90.8938	81.6569	89.2537	89.8859	89.3606
O1FeN5	NA	NA	NA	175.6874	NA	167.8485

Table 4.8: The angle of the first coordination sphere of iron complexes

On the other hand, *L3* and *L4* complexes show that due to L3 chlorine dioxide does not form a covalent coordination bond with the metal center, the geometry of it is a square base pyramid geometry. Contrary to *L3′*, its geometry is octahedral because the chlorine dioxide, in this case, is coordinated to iron as an axial ligand. The same effect is observed in the case of the *L4′* complex.

Another remarkable structural aspect of the L3 and L3' complexes is that the distortion evidenced in all other complexes, is not observed in this case, here the macrocyclic ring keeps planar as L0 complex.

On the other hand, an important structural parameter is the length of the iron to the ligand. Previously, its measurement was presented; however, it is not the case for some complexes as L1, L4, and L3 due to those not forming a coordination bond with the metal center. As summarized in table 4.10 here, we can observe that the complexes which do not present a coordination bond are major to 2 Å of distance, and the simple bond is $1.5 - 1, 7$ Å. As a result, only the complexes L2, L3', and L4' get to coordinate to the metal center and form a sixth ligand.

Complex	Atoms	Length (Å)
L1	Fe-O	2,0453
L2	Fe-O	1,7633
L3	Fe-Cl	2,5680
L3'	Fe-O	1,8990
L4	Fe-Cl	2,5452
L4'	Fe-O	1,8991

Table 4.9: Length between ligand and iron

4.1.7 Electronic Properties

Analysis of ligands

The iron complexes studied were proved with different distal ligands water, oxygen, chlorine dioxide, and chlorite ion. The optimization geometry of those shows the energy difference being the most greater negatively oxygen and chlorine ion followed by chlorine dioxide and water (Table 4.10).
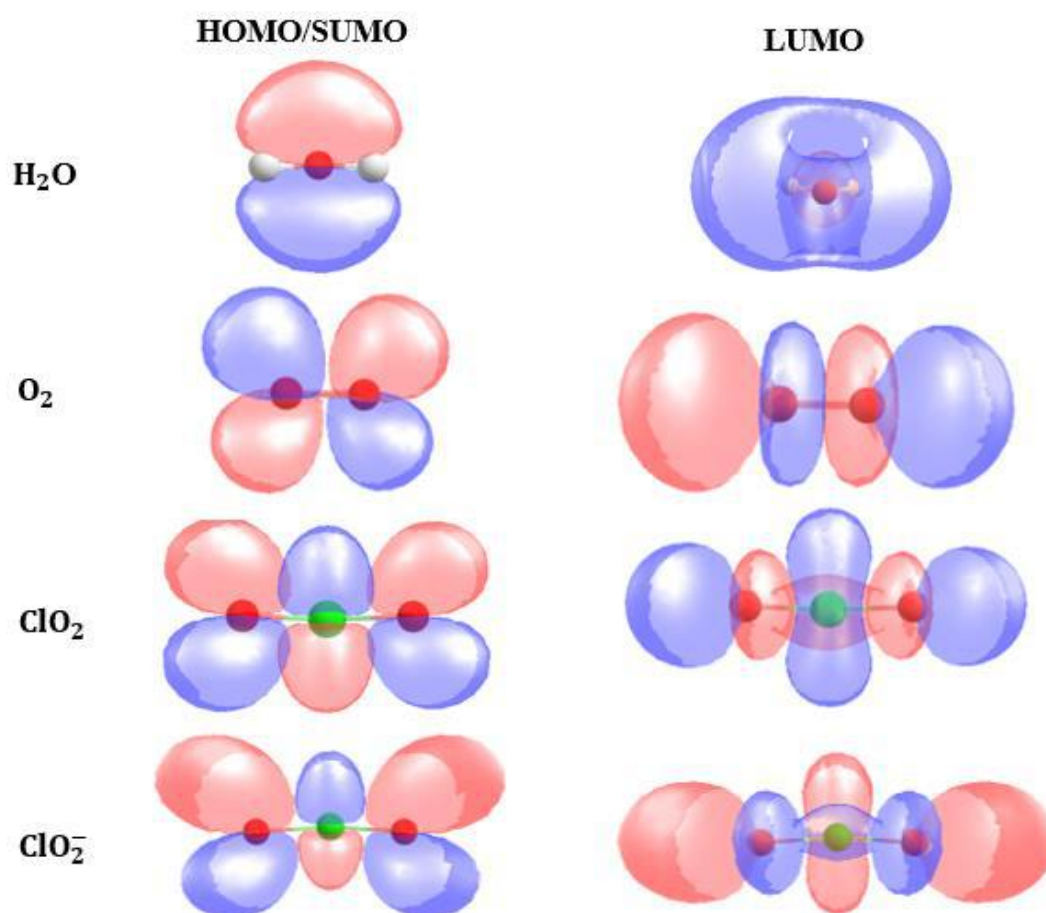
Figure 4.7: Molecular Orbitals of ligands

Ligand	Energy (Eh)	Energy (KJ/mol)	HOMO (ev)	LUMO (eV)
H_2O	-76.3217	-200382.7339	-7.8328	1.2781
O_2	-3718.4028	-9762667.1704	-8.2729	6.1732
ClO_2	-610.0394	-1601658.5210	-7.6091	-0.6876
ClO_2^-	-610.0889	-1601788.4969	1.5965	6.8605

Table 4.10: Energy of optimization geometry and HOMO, SUMO, and LUMO orbitals

The frontier molecular orbital analysis of four ligands offers significant information about them (Figure 4.7). In the case of energies of water, dioxygen and chlorine ion

are $-7.8328, -8.2729$, and 1.5965 ev for HOMO and -7.6091 ev for SUMO in the case of chlorine dioxide; while the LUMO energies are $1.2781, 6.1732, -0.6876, 6.8605$ ev for water, oxygen, chlorine dioxide, and chlorine ion respectively.

Analysis of iron complexes

The electronic properties analysis of the iron complexes studied is essential in the comprehension of the reactivity of these molecules. Table 4.11 shows some properties obtained through HOMO and LUMO orbitals. The bandgap energy values demonstrate how it decreases being the minimum when heme is coordinated to ClO_2 and ClO_2^-, which means that the reaction between those ligands is stronger than water and oxygen interactions.

	L0	**L1**	**L2**	**L3'**	**L4'**
HOMO	-8,2361	-8,3659	-8,6174	-8,3237	-5,6717
LUMO	-7,4660	-7,4595	-7,559	-7,0753	-4,5345
$E_G(ev)$	-0,7701	-0,9064	-1,0585	-1,2484	-1,1371
I (ev)	8,2361	8,3659	8,6173	8,3237	5,6717
EA (ev)	7,4660	7,4595	7,5588	7,0752	4,5345
$\mu(ev)$	-0,3850	-0,4532	-0,5292	-0,6242	-0,5685
$\eta(ev)$	0,3850	0,4532	0,5292	0,6242	0,5686

Table 4.11: Electronic properties of iron complexes

Another property is the ionization potential, the highest energy value is $8,6174$ ev corresponding to the complex L2, while the lowest value is $5,6717$ ev corresponding to the L4' complex. The decreased values of ionization potential indicate that of the four ligands, oxygen needs more energy to catch an electron of the valance shell of the iron while chlorite ion does it more easily; for this reason, it ligand requires less energy.

Therefore, the electron affinity values are similar in L0, L1, L2, and L3', but a drastic change is an evidence in L4', being the complex with the lowest electron affinity energy. Then, the chemical potential increases negatively in the order L0, L1, L2, L4' and L3'. These properties show that there is a major electronic flow between those ligands and the heme group. The last electronic property analyzed is the chemical hardness, another way to measure the molecular reactivity in terms of resistance to change the electronic distribution of the system, so the reported values of chemical hardness show how the reactivity of the complexes studied a range of $0,3850 - 0,6087$ begging the most reactive complex L4' and L3'.

Those previous electronic properties, help us to understand the reactivity of the molecules. Their general behavior of them shows that L3' and L4' are complex with major reactivity, conferring by the boundaries orbitals HOMO and LUMO in the case of L0, L1, L2, and L4' and SUMO and LUMO for the case of L3' (Figure 4.8).
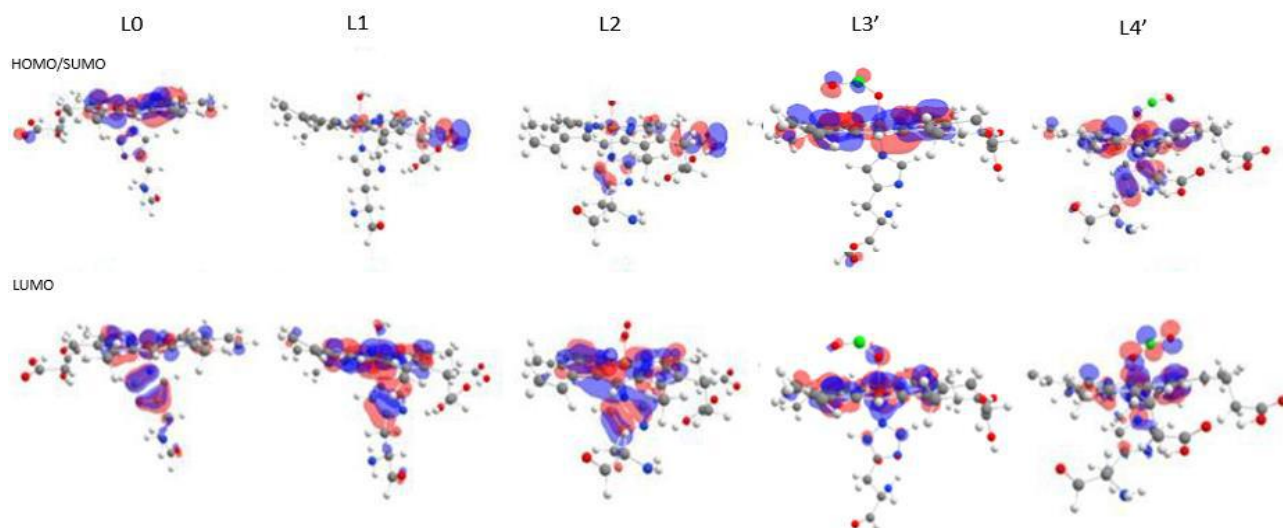
Figure 4.8: HOMO, SUMO, and LUMO of L0, L1, L2, L3' and L4' complexes

Based on the electronic properties is possible to establish an order of affinity of the ligands being $ClO_2^- > ClO_2 > O2 > H_2O$

4.2   Experimental Results

4.2.1   Purification of CAT-2 and Electrophoresis

The CAT-2 enzyme, expressed in E.coli was used as our heme-b source, so the purification of it was the main step to carry out further studies. The efficient purification was possible to make with affinity chromatography of Ni-NTA, the enzyme was labeled with a chain of six histidines. This method does that to the moment to load the sample to the column, the CAT-2 interacts with the Ni^{+2} and as consequence its time retention increase leaving elute the protein remains that could be in the samples.

The electrophoresis shows that this method of purification was efficient; however, the protein residues of low weight were not removed totally. In order to improve the purification method, a subsequent molecular exclusion chromatography was performed (Figure 4.9), indeed the presence of a second protein with almost the same retention time was obtained, the resolution of both enzymes CAT-2 and the second protein

designated as modified-CAT-2, m-CAT-2, was enough to obtain a purer fraction of CAT-2.
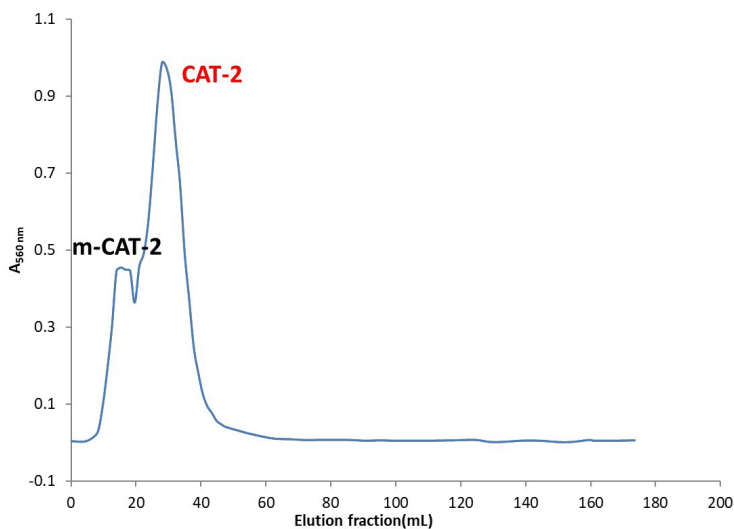
Figure 4.9: Chromatogram of the purification of CAT-2 by molecular exclusion chromatography

As we can see in figure 4.10 which corresponds to the SDS-PAGE gel after the chromatography in all bands of the different fractions appear a clear band between 72-95 kDa, which corresponds to the monomer CAT-2 of molecular weight of 84 kDa, and the other appears between 130-200 kDa which correspond to the dimmer of CAT-2. It is worth noting that the second chromatographic step by molecular exclusion, indeed increases the purity of CAT-2.

4.2.2   Protein Quantification

The Bradford method was applied to serial dilution of the BSA standard protein, which let us draw the standard calibration curve, through the treatment with Bradford reagent (Coomassie blue), that by electrostatic and Van der Waals interactions it binds to the protein, evidencing a color change of red (without protein) to blue (protein present). Furthermore, the intensity of the coloring is directly related to the protein concentration. For this reason, to know the protein concentration their absorbance was measured.

Once getting the standard curve calibration, as we can see in figure 4.11, through the lineal equation obtained is possible to calculate the concentration of the samples. Table 4.12 shows the absorbance and concentration determined to the samples only CAT-2, and the fractions (F) 1, 2, 2B, and 3. The major protein concentration was
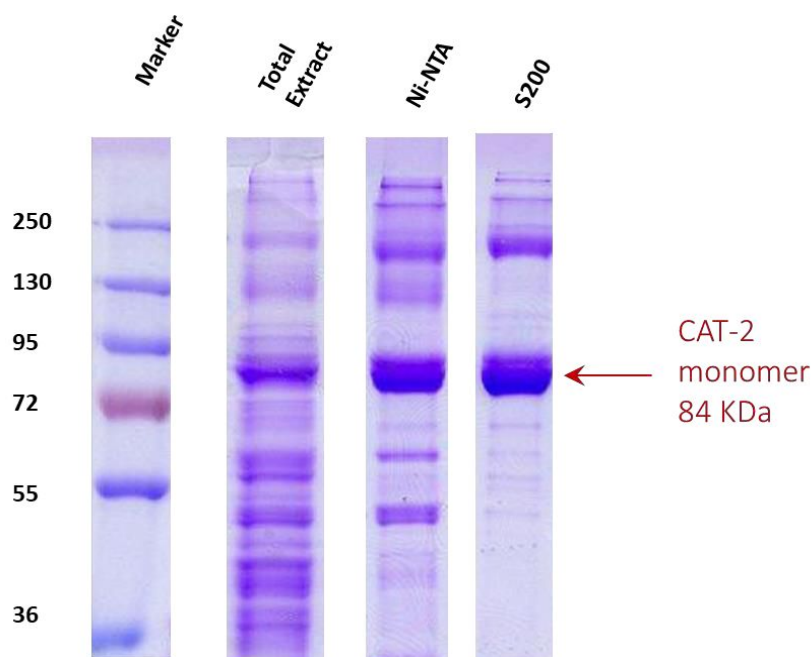
Figure 4.10: SDS-PAGE gel after Ni-NTA and S-200 chromatography purification
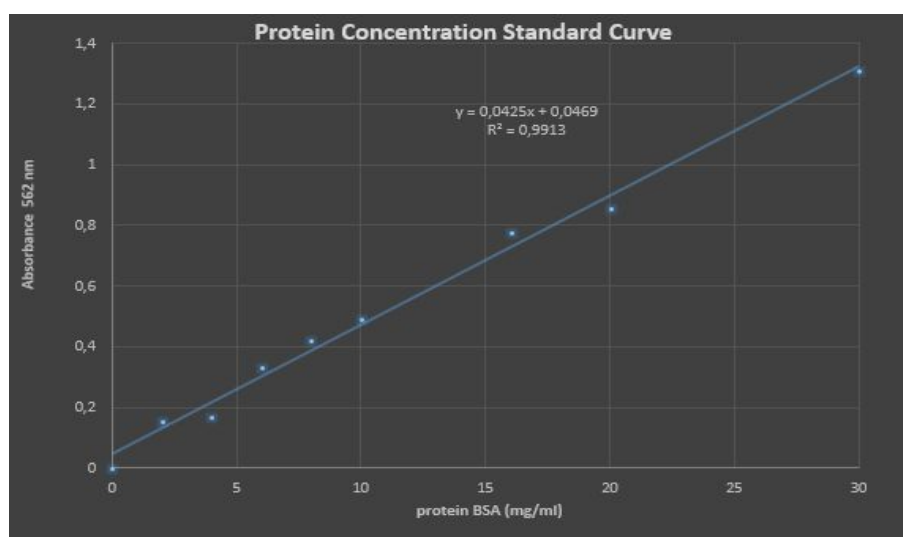
Figure 4.11: Protein Concentration Standard Curve

determined in fractions 1,µg.40,4 μg.

On the other hand, the major protein concentration of the different fractions is given by CAT-2 which is in agreement with the electrophoresis results; however, we know that there is the presence of other protein residues in less quantity; as consequence, in the quantification of Bradford assay, those residues are considered because reacting with the Coomassie blue too. For this reason, with the exception of only the CAT-2 sample, the rest of the fractions analyzed are a good approach to the CAT-2 content.

Sample	Protein (μg)	Concentration ($\mu g/mL$)
CAT-2	28.1	14.04
F1	40.4	20.19
F2	4.8	2.42
F2B	5.0	2.61
F3	6.3	3.15

Table 4.12: Protein concentration by Bradford standard curve

4.2.3   Reaction CAT-2 with ClO$_2$

In order to know the influence of the chlorine dioxide with the heme-b group, a commercial solution of it was put in contact with CAT-2, our heme source, the solution was analyzed by electronic spectroscopy. As we can see, figure 4.12 corresponds to the UV-Vis spectrum of the reaction of chlorine dioxide with CAT-2 (black) in comparison with the spectrum of the CAT-2 (red). The CAT-2 spectrum shows a pronounced peak at 281 nm, corresponding to the aromatic amino acids that according to the literature [79] the absorbance wavelength range (280-200)nm, this peak appears exactly at the same wavelength in CAT2-ClO_2 spectrum; however, the absorbance was decreased to 0,95 to 0,68.
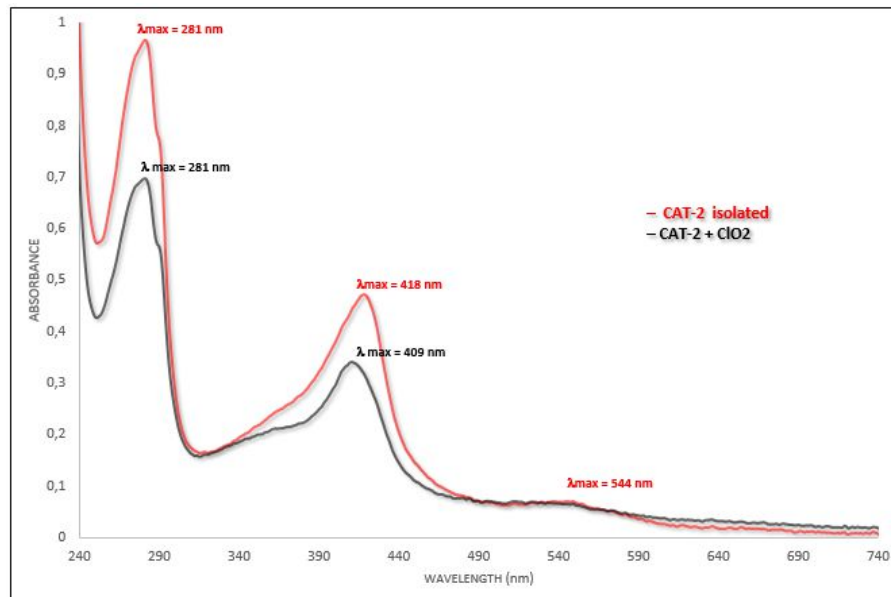
Figure 4.12: Electronic Spectroscopy of the CAT-2 isolate (red) and
CAT-2 interact with chlorine dioxide (black).

Therefore, to be a heme-b group in their oxidized form ($Fe^{+3}, 3d5$), and according to the Tanabe-Sugano diagram, we expected to observed three peaks corresponding to Soret band (γ), and two Q bands (α, β), in this case the Soret band due to electronic transitions between the $a_{1u} \rightarrow e_{gy}$ and $a_{2u} \rightarrow e_{gy}$ orbitals, while the Q bands are due to

$a_{1u} \rightarrow e_{gx}$ and $a_{2u} \rightarrow e_{gx}$. So in the CAT-2, spectrum Soret band appears at 418 nm and it is slightly shifted to the red region appearing at 409 nm in the CAT2-ClO_2 spectrum. The values are close to those reported in a range of (401-406) nm [64, 80]. Then, Q bands in both spectrums are not easy to observe; however we can see a maximum peak at 544 nm, and those bands were reported to appear in the region range of (500-600) nm [64, 81].

The reaction of ferric CAT-2 with commercial chlorine dioxide was very fast and the spectroscopic features mentioned above indicates that the chlorite present in commercial ClO2 don't have the capacity to oxidize ferric heme-b to Compound I (Fe(IV)=O), these result was verified by EPR results (data not shown) and such spectroscopic results look more like a probe of the heme degradation.

The reduction of CAT-2 with dithionite was carried out to compare with CAT2-ClO_2 spectrum and to prove if the phenomenon corresponds to a redox reaction. In this way, this method is considered a useful model system for investigating the effect of ligands on the redox properties of iron in a heme protein. Figure 4.13 corresponds to the spectrum of isolated CAT-2 spectrum (black) and CAT2-dithionite spectrum (blue). The reaction of the CAT-2 with dithionite results in the reduction of the heme-b group, which means that the metal center, iron becomes in ($Fe^{+2}, 3d^6$), and according to the Tanabe-Sugano diagram, three electronic transitions are expected to observe. The first one, the Soret band appear in 424 nm, which is close to the reported value of 428 nm, then the Q band are more visible in the reduction with dithionite and the band appears in 558 nm and 597 nm, alpha and beta peaks respectively; those values show similarity with those reported of 556 and 593 nm.

The peaks observed in each spectrum corresponds to specific electronic transitions of electron of HOMO to LUMO orbitals. These transitions can be determined using Tanabe-Sugano Diagrams as we can see in table 4.13.

Although the redox interaction was not proved by this method, an important effect caused by the chlorine dioxide is evidenced, the spectrum CAT 2 ClO2 indicated a degradation of the heme-b group due to the absorbance intensity decreased significantly in agreement with previously reported studies of the interaction of ferric myeloperoxidase and ferric lactoperoxidase [82].
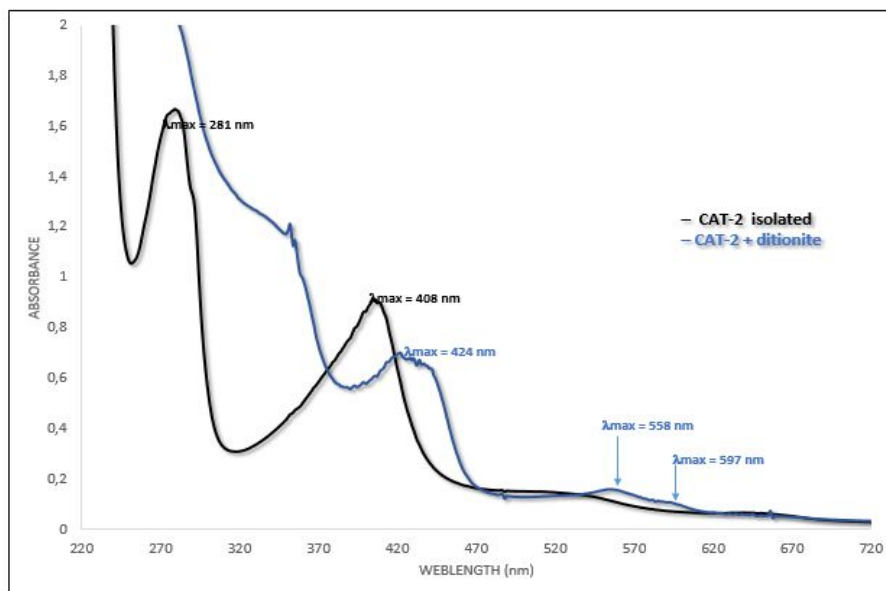
Figure 4.13: Electronic Spectroscopy of the CAT-2 isolate (black) and
CAT-2 reduced by dithionite (blue).

Spectrum	Electronic Transition
CAT-2	$^2T_2 \rightarrow^2 T_1$
	$^2T_2 \rightarrow^2 A_2$
	$^2T_2 \rightarrow^2 E$
CAT2-ClO2	$^2T_2 \rightarrow^2 T_1$
	$^2T_2 \rightarrow^2 A_2$
	$^2T_2 \rightarrow^2 E$
CAT2-ditionite	$^1A_1 \rightarrow^1 T_1$
	$^1A_1 \rightarrow^1 T_2$
	$^1A_1 \rightarrow^1 E$

Table 4.13: Electronic transition of spectrum CAT-2, $CAT2 - ClO_2$,
and CAT2-ditionite

Chapter 5

Conclusions and future work

- The optimization geometry of the complex $[Fe(ppIX)(his)]^+$ proved that it is more stable in a singlet state, which is in agreement with the literature due to deoxyhemoglobin which exhibits diamagnetic properties.

- The interaction of water molecules with the heme group produces a distortion in the square base pyramid; however, this ligand does not form a covalent bond.

- The ligand O2 forms the complex $[Fe(ppIX)(his)(O_2)]^+$ presenting a distorted octahedral geometry. The distortions correspond to saddling out of a plane

- Dioxide chloride molecule get to form the complex $[Fe(ppIX)(his)(ClO_2)]$ through oxygen iron bond of 1.8990 Å of distance and the single point energy show that it is a complex more stable than $[Fe(ppIX)(his)(H2O)]^+$.

- The computational analysis of the complexes studied indicated that chloride ion was coordinated to the iron through the oxygen atom; while the option of coordination through the chlorine atom was discarded due to the distance length of the ligand to the metal center is unable to form a coordination bond.

- The energy profile showed that chlorine dioxide and chloride ion are ligands that stabilized the complex $[Fe(ppIX)(his)]^+$ even more than which oxygen ligand. The greater negative values of the energy give an idea of the affinity of the heme group for the ligands, ranged in increase affinity order; $ClO_2^- > ClO_2 > O_2 > H_2O$.

- Through Mulliken Analysis Population was possible to determine that indeed when chloride dioxide gets to coordinate to the heme group the electronic density of the iron change, it decreased significantly, and the approximation values of the oxidation stated showed that there is oxidation by the action of those ligands.

- The major stability of the $[Fe(ppIX)(his)(ClO_2)]^+$ against $[Fe(ppIX)(his)(O_2)]^+$, and the electronic density changes by the action of the ClO_2 gives us an idea of

the future health problems that it could produce due to alters the functionality of the heme-b group doing it unable to bind oxygen.

- Chlorine dioxide is coordinated to iron forming the complex $[Fe(ppIX)(his)(ClO2)]^+$ through the oxygen atom. This complex is energetically more stable than the complex which interacts with iron through chloride atoms.

- The electronic properties of the complexes proved that those with chlorine dioxide and chlorine ion as distal ligands are most reactive than those with water and oxygen.

- The presence of the CAT-2 enzyme after the purification of a cell extract of E.coli M15/pREP4 strain was determined by the electrophoresis technique, where monomer and dimmer of CAT-2 appear in the range of (72-95) kDa and (130-200)kDa respectively, which is in agreement to the molecular weight reported. The extra molecular exclusion step improves the purification method of the enzyme.

- The treatment of the CAT2 with chlorine dioxide solution does not produce a redox reaction; however, it produces a degradation of the heme-b group, which was evidenced by the decreased absorbance intensity.

- The degradation of the heme-b group by the presence of chlorine dioxide suppose a severe health problem, due to the loss of it implies a disability of the enzymatic biological functions.

- The computational study is in agreement with the experimental results, due to theoretically the heme b complex does not change dramatically in terms of its electronic properties when it is coordinated with ClO_2, while experimentally does not occurs a redox reaction. However, it can be of concern for health that there is a better affinity with ClO_2 than with O_2.

Future Work

Through this study was possible to understand some important effects of chlorine dioxide in the role of the heme-b group, which implies damage of its functions. However, is necessary to do experimental studies with different chlorine concentrations to which let us corroborate the oxidation of iron in heme previously reported. Therefore, is important to do characterization of the complex $[Fe(ppIX)(his)(ClO2)]^+$ to prove the computational result about the coordination of chlorine dioxide and chlorite by an oxygen atom. In addition, corroborate the UV-Vis spectrum with a simulation by TD-DFT.

Appendix A

Coordination Chemistry of Iron

The complex conforms by heme group, histidine and oxygen, which is the active site of the hemoglobin, can be described from the point of view of the different theories as Valance Bond, Crystal field and Molecular Orbital Theories.

A.0.1   Valance Bond Theory

From of point of view of the valance bond theory the formation of the complex involves the reaction between Lewis bases (ligands) and Lewis acid (metal center) [53]. This theory lets us explain the formation of hybrid orbitals and predict magnetic properties as well as geometry.

Figure A.1a shows the scheme of valance bond for ferrous ion complex in which exhibits the two possible cases of electron arrangement, both with octahedral geometry but with different magnetic properties. In the same way, figure A.1b shows the scheme of valance bonds for the ferric complex. In this case, the geometry does not change in comparison with ferrous ions, but the two cases exhibit paramagnetic properties.

Base on the diagram of the valance band, both ferrous and ferric complex presents an octahedral geometry; however, the magnetic properties to change depends on the arrangement of the electrons. According to the previous studies it was found that hemoglobin has magnetic properties that are different depending on whether it is carrying oxygen or not when the hemoglobin is not carrying oxygen has 5.46 Bohr magnetons (B.M.) [54] which are only slightly larger than the 4.90 B.M. value expected for four unpaired spins per Fe(II) based on a spin-only formula. Therefore, when hemoglobin is bound to oxygen it is a diamagnetic molecule.
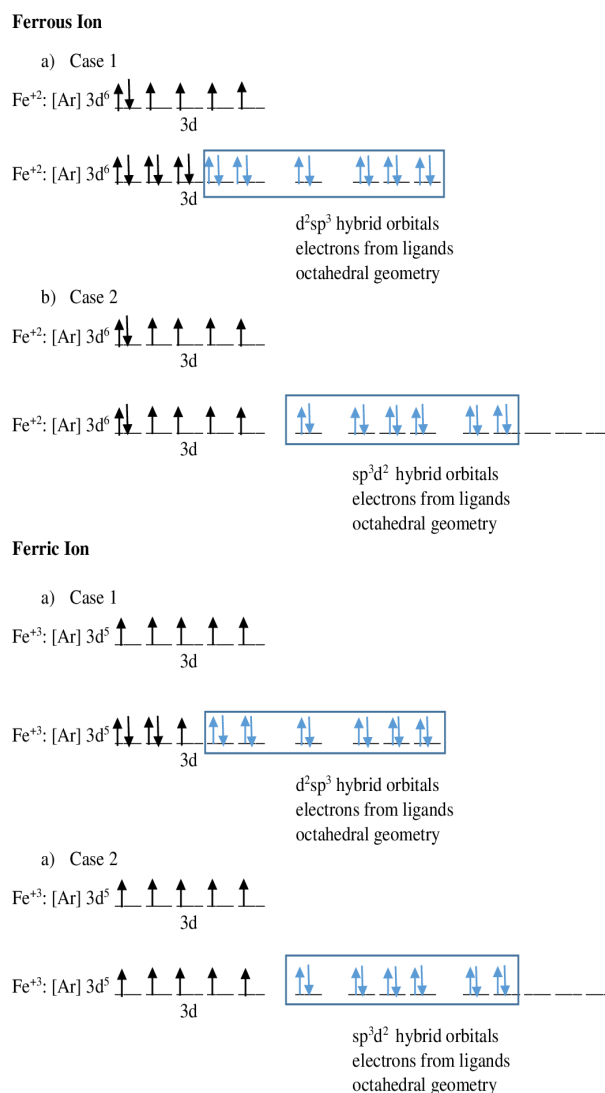
Ferrous Ion

   a) Case 1

Fe^{+2}: [Ar] $3d^6$

          3d

Fe^{+2}: [Ar] $3d^6$

          3d

                  d^2sp^3 hybrid orbitals
                  electrons from ligands
                  octahedral geometry

   b) Case 2

Fe^{+2}: [Ar] $3d^6$

          3d

Fe^{+2}: [Ar] $3d^6$

          3d

                sp^3d^2 hybrid orbitals
                electrons from ligands
                octahedral geometry

Ferric Ion

   a) Case 1

Fe^{+3}: [Ar] $3d^5$

          3d

Fe^{+3}: [Ar] $3d^5$

          3d

                  d^2sp^3 hybrid orbitals
                  electrons from ligands
                  octahedral geometry

   a) Case 2

Fe^{+3}: [Ar] $3d^5$

          3d

Fe^{+3}: [Ar] $3d^5$

          3d

                sp^3d^2 hybrid orbitals
                electrons from ligands
                octahedral geometry

Figure A.1: Valance Bond scheme for ferrous and ferric ions

A.0.2 Crystal Field Theory

Considering the octahedral geometry for the ferrous and ferric complex given by the valance bond is possible to predict the splitting to the octahedral field through the crystal field theory, which postulates that there is an spherical hypothetical field in which d orbitals are not perturbing due to the absence to the ligands, but when appearing the electrostatic interactions between the ionic central and ligands, those produce that d orbitals degeneration.

One of the most important parameters to consider in the field splitting is the nature of the ligands, so in the case of the heme group, the ligands are porphyrin ring, histidine, and oxygen or the substrate. In figure A.2 we can observe the two most common cases of high spin and low spin for the ferric and ferrous ions; however, iron
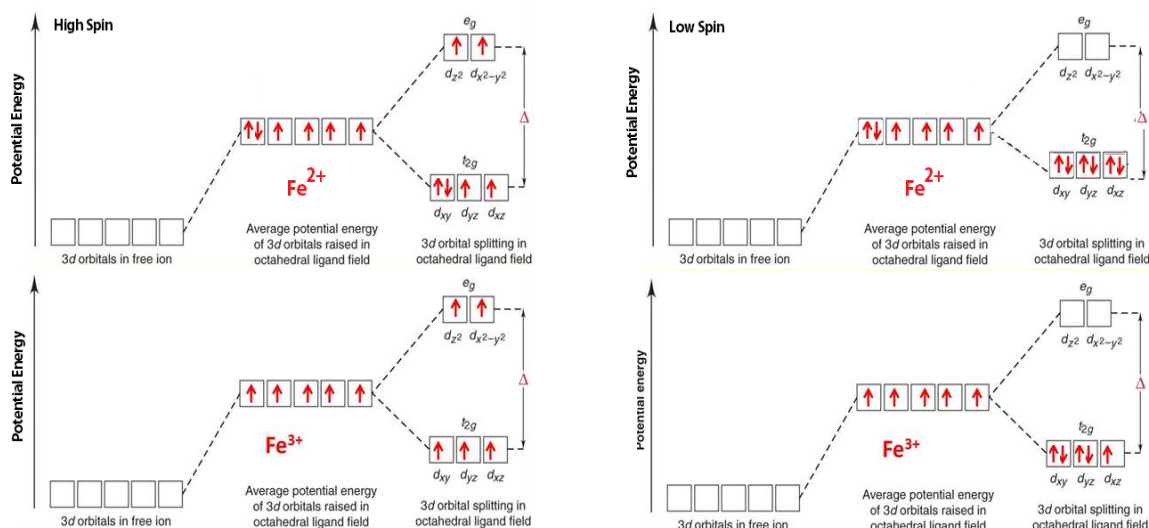
Figure A.2: Cristal Field diagram for ferric and ferrous ions in high
and low spin

ions exhibit another spin state less common. Now, is well known that there are some factors that affect how the field is splitting, between them is the nature of the ligand. Base on data for a wide variety of complexes, it is possible to list ligands in order to increase field strength in a spectrochemical series [53].

A.0.3 Molecular Orbital Theory

Molecular Orbital Theory (MOT) is an approach in the understanding of the bonding in molecules by combining atomic orbitals of the atoms which form the molecule [53]. The interaction of two orbitals produces two news, each one with different energies, those with major energy value are considered bonding orbitals, while those with less energy are anti-bonding orbitals [83]. Generally, the interactions are given by Highest occupied molecular orbital (HOMO) and lowest unoccupied molecular orbital (LUMO), those are denominated as boundary orbitals [84].
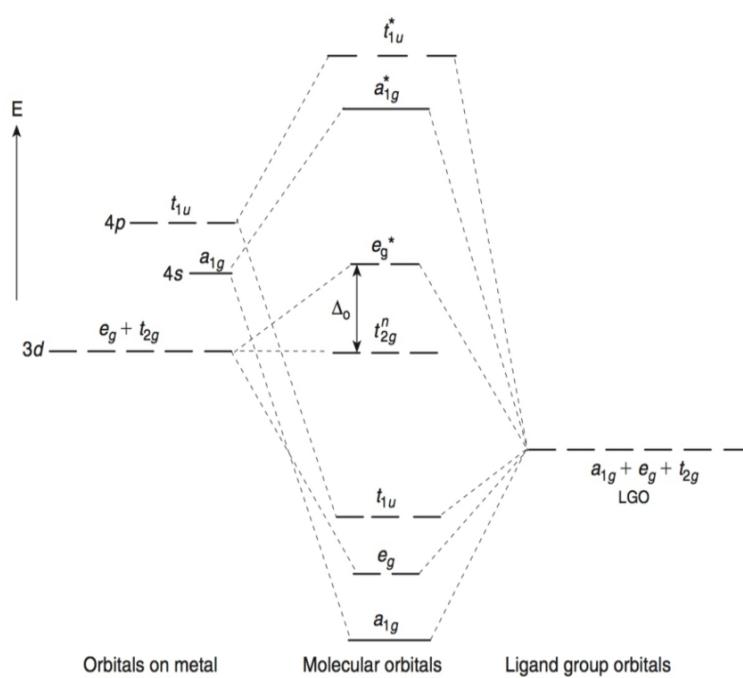
Figure A.3: Molecular orbitals of an octahedral complex. The figure
is taken from Ref. [85]

Bibliography

(1) Organization, W. H. WHO Director-General's opening remarks at the media briefing on COVID-19, https://www.who.int/dg/speeches/detail/who-directorgeneral-s-opening-remarks-at-the-media-briefing-on-covid-19---11-march-2020, 2020.

(2) Lardieri, A.; Cheng, C.; Jones, S. C.; McCulley, L. *Clinical toxicology (Philadelphia, Pa.)* **2021**, *59*, 448.

(3) Loh, J. M. R.; Shafi, H. *Case Reports* **2014**, *2014*, bcr2014205832.

(4) Hernández, R. G. *Medimay* **2014**, *5*, 41–50.

(5) Deininger, R.; Ancheta, A; Ziegler, A *University of Michigan. Escuela de Salud Pública. The University of Michigan* **1998**.

(6) Vilca Maquera, G. N. **2017**.

(7) Chen, Y.-S.; Vaughn, J. M. *Applied and environmental microbiology* **1990**, *56*, 1363–1366.

(8) Kuhne, F. W. Use of a chemically-stabilized chlorite matrix for the parenteral treatment of HIV infections, US Patent 6,086,922, 2000.

(9) Rehr, A.; Jansen, M. *Angewandte Chemie International Edition in English* **1991**, *30*, 1510–1512.

(10) CAVERO, V. *CON CIENCIA* **2020**, *8*.

(11) Masschelein, W. *Chemical Oxidation: Technology for the Nineties, Volume I* **2021**, 170.

(12) Taylor, J. B., *Toxicological profile for chlorine dioxide*; Diane Publishing: 2010.

(13) Ueno, H.; Sayato, Y.; Nakamuro, K. *Journal of health science* **2000**, *46*, 110–116.

(14) Gordon, G.; Kieffer, R. G.; Rosenblatt, D. H. *Progress in inorganic chemistry* **1972**, *15*, 202–286.

(15) García Afanador, M.; Castro, C. G. **2011**.

(16) Trinetta, V; Morgan, M; Linton, R In *Microbial Decontamination in the Food Industry*; Elsevier: 2012, pp 533–562.

(17) Gordon, G.; Rosenblatt, A. A. *Ozone: science & engineering* **2005**, *27*, 203–207.

(18) Insignares, E; Bolaño, B; Andrade, M; Matos, C; Aparicio, M.; Chavez, P; Velazquez, R; Pelizari, D; Montelongo, E; Fontana, R, et al.

(19) Mynenivenkatasatya, S. R.; Wang, H.; Cooley, W.; Garcia-Smith, E.; Shewale, J.; Ratcliff, J. *Dentistry journal* **2020**, *8*, 122.

(20) Couri, D; Abdel-Rahman, M. *Journal of environmental pathology and toxicology* **1979**, *3*, 451–460.

(21) García, R; Sarmiento, C *AEMEMI* **2020**.

(22) Kalcker, A., *Salud Prohibida Incurable Era Ayer*; Voicedialogo. España: 2016.

(23) Akamatsu, A.; Lee, C.; Morino, H.; Miura, T.; Ogata, N.; Shibata, T. *Journal of Occupational Medicine and Toxicology* **2012**, *7*, 1–8.

(24) Condie, L. W. *Journal-American Water Works Association* **1986**, *78*, 73–78.

(25) Dalhamn, T et al. *Arch. Indust. Health* **1957**, *15*, 101–7.

(26) Bercz, J.; Jones, L; Garner, L; Murray, D; Ludwig, D.; Boston, J *Environmental health perspectives* **1982**, *46*, 47–55.

(27) Abdel-Rahman, M.; Couri, D; Bull, R. *Journal of environmental pathology, toxicology and oncology : official organ of the International Society for Environmental Toxicology and Cancer* **1985**, *6*, 105—113.

(28) MORINO, H.; FUKUDA, T.; MIURA, T.; LEE, C.; SHIBATA, T.; SANEKATA, T. *Biocontrol science* **2009**, *14*, 147–153.

(29) For Toxic Substances, A.; (ATSDR), D. R. *Applied and environmental microbiology* **2004**.

(30) Abdel-Rahman, M.; Couri, D; Bull, R. *Journal of the American College of Toxicology* **1984**, *3*, 269–275.

(31) Couri, D.; Abdel-Rahman, M. S.; Bull, R. J. *Environmental Health Perspectives* **1982**, *46*, 13–17.

(32) Ueno, H.; Sayato, Y.; Nakamuro, K. *Journal of health science* **2000**, *46*, 110–116.

(33) Storz, J. F., *Hemoglobin: insights into protein structure, function, and evolution*; Oxford University Press: 2018.

(34) Alvarez-Paggi, D.; Hannibal, L.; Castro, M. A.; Oviedo-Rouco, S.; Demicheli, V.; Tortora, V.; Tomasina, F.; Radi, R.; Murgida, D. H. *Chemical reviews* **2017**, *117*, 13382–13460.

(35) Layer, G. **2020**.

(36) Collins, D.; Dawson, J. **2013**.

(37)   Shelnutt, J.; Medforth, C., et al. *Chemical Society Reviews* **1998**, *27*, 31–42.

(38)   Jain, R.; Chan, M. K. *JBIC Journal of Biological Inorganic Chemistry* **2003**, *8*, 1–11.

(39)   Olea Jr, C.; Boon, E. M.; Pellicena, P.; Kuriyan, J.; Marletta, M. A. *ACS chemical biology* **2008**, *3*, 703–710.

(40)   Kingsbury, C. J.; Senge, M. O. *Coordination Chemistry Reviews* **2021**, *431*, 213760.

(41)   Hobbs, J. D.; Shelnutt, J. A. *Journal of protein chemistry* **1995**, *14*, 19–25.

(42)   Olea Jr, C.; Kuriyan, J.; Marletta, M. A. *Journal of the American Chemical Society* **2010**, *132*, 12794–12795.

(43)   Bikiel, D. E.; Forti, F.; Boechi, L.; Nardini, M.; Luque, F. J.; Marti, M. A.; Estrin, D. A. *The Journal of Physical Chemistry B* **2010**, *114*, 8536–8543.

(44)   Shin-ichi, J. T.; Ukpabi, G.; Murphy, M. E.; Mauk, A. G. *Proceedings of the National Academy of Sciences* **2011**, *108*, 13071–13076.

(45)   Coates, T. D. *Free Radical Biology and Medicine* **2014**, *72*, 23–40.

(46)   Xie, L. Y.; Dolphin, D. In *Metalloporphyrins catalyzed oxidations*; Springer: 1994, pp 269–306.

(47)   Heymsfield, S. B.; Waki, M.; Kehayias, J.; Lichtman, S.; Dilmanian, F. A.; Kamen, Y.; Wang, J; Pierson Jr, R. *American Journal of Physiology-Endocrinology And Metabolism* **1991**, *261*, E190–E198.

(48)   Abbaspour, N.; Hurrell, R.; Kelishadi, R. *Journal of research in medical sciences: the official journal of Isfahan University of Medical Sciences* **2014**, *19*, 164.

(49)   Mihailescu, M.-R.; Russu, I. M. *Proceedings of the National Academy of Sciences* **2001**, *98*, 3773–3777.

(50)   VERA, L. F. *Revista de la Real Academia de Ciencias Exactas Físicas y Naturales* **2010**, *104*, 213–232.

(51)   Thapaliya, B. P.; Dawadi, M. B.; Ziegler, C.; Perry, D. S. *Chemical Physics* **2015**, *460*, 31–42.

(52)   Gerloch, M. *Inorganic Chemistry* **1981**, *20*, 638–640.

(53)   Huheey, J. E.; Keiter, E. A.; Keiter, R. L.; Medhi, O. K., *Inorganic chemistry: principles of structure and reactivity*; Pearson Education India: 2006.

(54)   Bren, K. L.; Eisenberg, R.; Gray, H. B. *Proceedings of the National Academy of Sciences* **2015**, *112*, 13123–13127.

(55)   Xu, C.; Tobi, D.; Bahar, I *Journal of molecular biology* **2003**, *333*, 153–168.

(56) Palmer, A. F.; Belcher, D. A. In *Principles of Tissue Engineering*; Elsevier: 2020, pp 785–801.

(57) Subbiah, S; Silberstein, P. **2014**.

(58) Mansouri, A. *The American journal of the medical sciences* **1985**, *289*, 200–209.

(59) Walker, J. G.; Kadia, T.; Brown, L.; Juneja, H. S.; De Groot, J. F. *Journal of neuro-oncology* **2009**, *94*, 149–152.

(60) Svecova, D; Böhmer, D *Casopis lekaru ceskych* **1998**, *137*, 168–170.

(61) Benini, D; Vino, L; Fanos, V. *La Pediatria medica e chirurgica: Medical and surgical pediatrics* **1998**, *20*, 411–413.

(62) Jaffe, E. *Blood cells* **1986**, *12*, 81–90.

(63) Cortazzo, J. A.; Lichtman, A. D. *Journal of cardiothoracic and vascular anesthesia* **2014**, *28*, 1043–1047.

(64) Vega-García, V.; Díaz-Vilchis, A.; Saucedo-Vázquez, J. P.; Solano-Peralta, A.; Rudiño-Piñera, E.; Hansberg, W. *Archives of biochemistry and biophysics* **2018**, *640*, 17–26.

(65) Vazquez, N.; Ines, M., et al., *Algunos aspectos básicos de la química computacional*; UNAM: 2006.

(66) Lewars, E. *Introduction to the theory and applications of molecular and quantum mechanics* **2011**, 318.

(67) Suárez, D **2012**.

(68) Platas-Iglesias, C.; Roca-Sabio, A.; Regueiro-Figueroa, M.; Esteban-Gómez, D.; de Blas, A.; Rodríguez-Blas, T. *Current Inorganic Chemistry (Discontinued)* **2011**, *1*, 91–116.

(69) Koch, W.; Holthausen, M. C., *A chemist's guide to density functional theory*; John Wiley & Sons: 2015.

(70) Perdew, J. P.; Parr, R. G.; Levy, M.; Balduz Jr, J. L. *Physical Review Letters* **1982**, *49*, 1691.

(71) Foresman, J. B. Computational Chemistry: A Practical Guide for Applying Techniques to Real World Problems By David Young (Cytoclonal Pharmaceutics Inc.). Wiley-Interscience: New York. 2001. xxvi+ 382 pp. $69.95. ISBN: 0 − 471 − 33368 − 9., 2001.

(72) André, J.-M., *Exploring Aspects of Computational Chemistry: Concepts and Exercises 2 Volumes*; 2; Presses universitaires de Namur: 1997.

(73)   Ramos-Cordoba, E.; Postils, V.; Salvador, P. *Journal of chemical theory and computation* **2015**, *11*, 1501–1508.

(74)   Snyder, H. D.; Kucukkal, T. G. *Journal of Chemical Education* **2021**, *98*, 1335–1341.

(75)   Neese, F. *Wiley Interdisciplinary Reviews: Computational Molecular Science* **2018**, *8*, e1327.

(76)   Neese, F. *Wiley Interdisciplinary Reviews: Computational Molecular Science* **2012**, *2*, 73–78.

(77)   Tame, J. R.; Vallone, B. *Acta Crystallographica Section D: Biological Crystallography* **2000**, *56*, 805–811.

(78)   Vega, V. *Universidad Nacional Autónoma de México*.

(79)   Lavrinenko, I.; Vashanov, G.; Artyukhov, V. *Biophysics* **2015**, *60*, 197–204.

(80)   Cordova Torres, A. V. Study of High-Valent Iron Intermediates in biological and biomimetic systems, B.S. thesis, Universidad de Investigación de Tecnología Experimental Yachay, 2019.

(81)   Parra, Y.; Ferrer, R. E.; Montero, K.; Martínez, M. *Química Viva* **2011**, *10*, 154–186.

(82)   Jakopitsch, C.; Pirker, K. F.; Flemmig, J.; Hofbauer, S.; Schlorke, D.; Furtmüller, P. G.; Arnhold, J.; Obinger, C. *Journal of inorganic biochemistry* **2014**, *135*, 10–19.

(83)   Jean, Y., *Molecular orbitals of transition metal complexes*; OUP Oxford: 2005.

(84)   Zhuo, L.-G.; Liao, W.; Yu, Z.-X. *Asian Journal of Organic Chemistry* **2012**, *1*, 336–345.

(85)   House, J. E.; House, K. A., *Descriptive inorganic chemistry*; Academic Press: 2015.